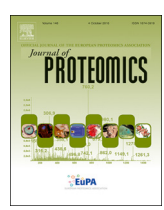
ELSEVIER

Contents lists available at ScienceDirect

Journal of Proteomics

journal homepage: www.elsevier.com/locate/jprot



Quantitative proteomic analysis of deer antler stem cells as a model of mammalian organ regeneration



Zhen Dong^{a,b}, Dawn Coates^b, Qingxiu Liu^c, Hongmei Sun^a, Chunyi Li^{a,d,*}

- ^a Institute of Special Wild Economic Animals and Plants, Chinese Academy of Agricultural Sciences, Changchun 130112, China
- ^b Sir John Walsh Research Institute, Faculty of Dentistry, University of Otago, Dunedin 9016, New Zealand
- ^c School of Medicine. Huagiao University. Quanzhou 362021. China
- ^d Changchun Sci-Tech University, Changchun 130600, China

ARTICLE INFO

Keywords: Regenerative medicine Deer Periosteum Antler stem cell Proteomics 2D-DIGE

ABSTRACT

The ability to activate and regulate stem cells during wound healing and tissue/organ regeneration is a promising field which could bring innovative approaches to regenerative medicine. The regenerative capacity of invertebrates has been well documented, however in mammals, stem cells that drive organ regeneration are rare. Deer antler is unique in providing a mammalian model of complete organ regeneration based on stem cells. The present study investigated the differentially regulated proteins (DRPs) between different antler stem cell populations (n=3) using 2D-DIGE. Western blotting was used to validate the proteomics results. Comparative proteomics resulted in protein profiles which were similar for the biological replicates but different between the cells derived from two different stem cell niches involved in antler growth/regeneration and cells derived from facial periosteum. Ninety-two up- and down-regulated proteins were identified by MALDI-TOF MS. The work indicates that the epithelial-mesenchymal transition process may participate in the initiation of antler regeneration including the first stage of scar-less wound healing. Cell mobility is also highly regulated during antler regeneration. Energy and nucleotide metabolism may however be less active in antler regeneration as compared to that in antler generation phase. These results provide new insights into the underlying mechanisms of stem cell-based regeneration of mammalian organs.

1. Introduction

Regenerative medicine aims to replace, engineer or regenerate new tissue, and by so doing to restore normal functioning to tissues or organs after lost-to-trauma or damaged by disease or aging [1]. Research in this field investigates an organism's own repair systems with the prospect of understanding how to functionally restore damaged tissues and organs [2]. Undoubtfully, this is the ultimate solution for the reestablishment of damaged or diseased tissues or organs and will ultimately offer a more meaningful alternative to xenotransplantation from animal organ donors which have multiple issues [3], including ethics, transplant rejection and the risk of cross-species disease transmission [4].

A major goal of regenerative research is to understand the molecular mechanisms directly associated with tissue and organ repair/regeneration. The discovery of a conserved and shared regenerative mechanism in animal models will assist the development of research lead therapies. A powerful example is that of the Wnt signaling pathway

which in both deer antler [5] and planarian [6], can reboot dormant or latent regenerative responses [7]. Animal models of regeneration can thus provide clues to how stem cells are maintained and activated.

Animal models of regeneration have been described in both invertebrates and vertebrates and result in either physiological or reparative regeneration. Regeneration driven from stem cells or attributed to the dedifferentiation or trans-differentiation of cells has been described in the literature [7,8]. Generally speaking, lower order animals have a higher regenerative potential and some invertebrate are capable of whole-body regeneration [8]. Deer antler is an example of physiological regeneration in a mammal [9], and offers the opportunity to study the regulation of a large stem cell niche responsible for driving growth at 1–2 cm/day. It is, actually, the only mammalian example of stem cell driven annual organ growth [10]. Antler regeneration is, at initial stage, a scar-less repair process which results in complete restoration of structure with function. Understanding the cellular mechanisms controlling this process could provide new approaches in regenerative medicine [7].

^{*} Corresponding author at: Institute of Special Wild Economic Animals and Plants, Chinese Academy of Agricultural Sciences, Changchun 130112, China. E-mail address: lichunyi1959@163.com (C. Li).

Z. Dong et al. Journal of Proteomics 195 (2019) 98–113

When a deer approaches puberty, antlerogenic periosteum (AP), which is found overlying the lateral crests of the deer frontal bone, develops first into a pedicle and then antler [11]. By transplanting the AP subcutaneously to deer nasal bone [11] or foreleg [12], ectopic antlers have been successfully induced. More surprisingly, when AP was grafted on the head of a nude mouse it produced pedicle-like [13], and even antler-like [14] bony protuberances. After casting of the first-years antler, it is the pedicle periosteum (PP) around the permanent bony protrusion on the deer skull that induces subsequent regrowth of antler. This has been confirmed by depletion of the PP overlying the bone, which results in the loss of antler regeneration [15]. Based on the degree of contact between the PP and the enveloping skin, the proximal two-thirds of the pedicle is referred to as the "dormant PP" (DPP) while the distal third is referred to as the "potentiated PP" (PPP) [16]. AP/PP cells (APCs/PPCs), antler stem cells residing in periosteum, express key embryonic stem cell markers and have been induced into multiple cell types, such as chondroblasts, adipocytes, osteoblasts, muscle precursor cells and neuronal-like cells [17-20]. In addition, the mesenchymal/ epithelial interactions between the AP/PP and the enveloping skin are essential for the initiation of antler generation/regeneration. Velvet skin may contribute to the niche which is important for the maintenance and regulation of antler stem cells [20].

Two-dimensional difference gel electrophoresis (2D-DIGE) is a two-dimensional electrophoresis-upgraded and fluorescent dye-labeled quantitative proteomics. The use of an internal pooled standard can increase the quantification accuracy and statistical confidence [21]. The multivariable statistical analyses before mass spectrometry filters out the noise from technical and biological variations in order to concentrate on the underlying differences that reflect various disease or biological states [22]. Currently, it remains unclear how the APCs, DPP cells (DPPCs) and PPP cells (PPPCs) are regulated at molecular level. The present study investigated the DRPs through 2D-DIGE, and the activated signaling pathways through bioinformatic analysis of different types of antler stem cells and facial periosteum cells (FPCs) derived from the nasal bone on the deer head as the control. This study aimed to elucidate the proteins and molecular mechanisms controlling stem cell during mammal organ regeneration.

2. Material and methods

2.1. Tissue sampling and primary cell culture

AP, PPP, DPP and FP (n = 3/tissue type) were harvested from sika

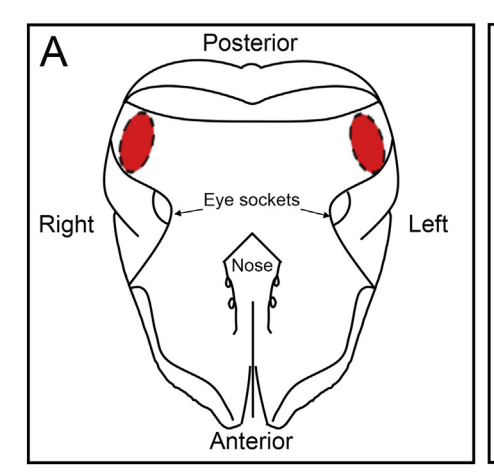
deer (Cervus nippon) heads (Fig. 1) immediately after slaughtering in October and May respectively, under approval from the Animal Ethics Committee at the Institute of Special Wild Economic Animals and Plants, Chinese Academy of Agricultural Sciences (Permit Number: CAAS2015020), using the method previously described by Li and Suttie [16]. The primary cell culture for all tissues was conducted following established protocols [23,24]. Briefly, each periosteum sample was cut into small pieces using two scalpels in a petri dish and digested in DMEM medium (Life Technologies, USA) containing 150 U/mL collagenase (Invitrogen, USA). Cells were then collected and grown in culture medium consisting of DMEM medium with 10% FBS (Gibco, USA), 100 U/mL penicillin and 100 µg/mL streptomycin. Cells were trypsinized when becoming sub-confluent, transferred into T75 culture flasks (Nest Biotechnology, China), and grown until there were 1×10^5 cells/mL. Cryopreservation was conducted in freezing medium (FBS + 10% DMSO; Sigma, USA) and cells stored in liquid nitrogen.

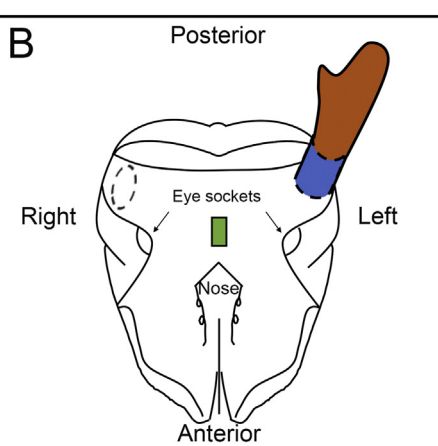
Harvested cells were not further purified into sub-populations as it is currently unknown whether a single stem cell type or all cell types of periosteum tissue are necessary for antler generation and regeneration. Cells were retrieved from storage and grown in the culture medium to sub-confluence (around 85%) in T75 flasks prior to use.

2.2. Protein extraction and labeling

After decanting the culture medium from the T75 flasks, cells were trypsinized, centrifuged and re-suspended in cell wash solution (10 mM Tris (GE Healthcare, USA), 5 mM magnesium acetate (Sigma, USA), 1 mM PMSF (Roche, Switzerland)), centrifuged and washed again. The cell pellet was then re-suspended in 550 μ L lysis buffer (7 M Urea, 2 M Thiourea, 30 mM Tris, 4% (w/v) 3-[(3-Cholamidopropyl) dimethylammonio]-1-propanesulfonate (CHAPS), and 10 μ L/mL protease inhibitor cocktail; GE Healthcare, USA). A Bullet Blender (Next Advance, USA) was used at the 7th level for 1 min to break the cells after the addition of stainless steel beads (0.5 mm in diameter; 0.5:1.0 ratio in volume of beads to lysis buffer). The homogenates were solubilized by incubating for 3 h on ice with shaking, before centrifuging at 12,000 g and 4 °C for 15 min. The supernatants were collected, aliquoted and stored at -80 °C.

Supernatants (50 μ L) from each sample were cleaned and precipitated using a 2D Clean-up kit (GE Healthcare, USA), and pellets resuspended in 50 μ L lysis buffer (7 M Urea, 2 M Thiourea, 30 mM Tris, 4% (w/v) CHAPS, pH 8.5). Protein concentration was measured using a RC DCTM Protein Assay (Bio-Rad, USA). Proteins were labeled with





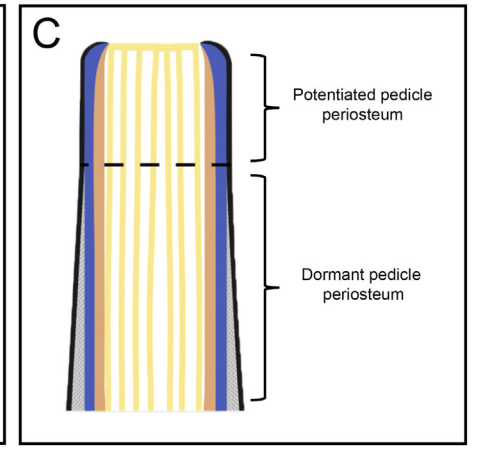


Fig. 1. Tissue sampling. When a deer reaches puberty, antlerogenic periosteum (A; red), which is situated over the frontal bone, grows into a bone protrusion, called pedicle, and this subsequently forms the first-year antler (B; Brown). The periosteum around the pedicle is called pedicle periosteum (B & C; Blue) and is characterized based on the degree of contact between the periosteum and enveloping skin. The distal third is tightly attached and referred to as potentiated pedicle periosteum; the proximal two thirds are loosely attached and called dormant pedicle periosteum (C). Facial periosteum (B; Green) over the nasal bone between the two eye sockets was used as the control. (For interpretation of the references to colour in this figure legend, the reader is referred to the web version of this article.)

CyDye DIGE Fluor minimal dyes (GE Healthcare, USA) following the manufacturer's instructions. CyDye (1 μ L at 400 pmol) was added to 50 μ g of protein from each sample and incubated on ice in the dark for 30 min. The samples were labeled with Cy3 and Cy5 respectively, and the internal standard was made by mixing equal amounts (4.17 μ g) of protein from each sample and labeling with Cy2. After incubation with the labels the reactions were stopped by adding 1 μ L of 10 mM lysine (Sigma, USA) solution.

2.3. Two-dimensional differential gel electrophoresis

An equal volume of 2× sample buffer (DeStreak™ Rehydration Solution, 2% IPG buffer, 20 µL/mL protease inhibitor cocktail; GE Healthcare, USA) was added and 24 cm pH 3-10 Non-Linear (NL) dry stripes (GE Healthcare, USA) were rehydrated for 14 h using the IPGbox and IPGbox kit (GE Healthcare, USA). Isoelectric focusing (IEF) was performed at 20 °C in an Ettan™ IPGphor 3 (GE Healthcare, USA), using the following program: 250 V for 250 Vh, 500 V for 500 Vh, 500-1000 V for 800 Vh, 1000-6000 V for 8000 Vh, 6000-10,000 V for 8500 Vh, 10,000 V for 34,700 Vh, and 500 V for 1 h. Strips were then equilibrated for 15 min in 10 mL reducing solution (6 M urea, 50 mM Tris-HCl pH 8.8, 30% v/v glycerol, 2% w/v SDS and 50 mg DTT; GE Healthcare, USA), followed by 15 min in 10 mL alkylating solution (6 M urea, 50 mM Tris-HCl pH 8.8, 30% v/v glycerol, 2% w/v SDS and 450 mg iodoacetamide; GE Healthcare, USA) in the dark. The protein separation in the second dimension was carried out on an Ettan DALTsix unit (GE Healthcare, USA) with 12.5% polyacrylamide gels. Electrophoresis was run at 22 °C, 2 W/gel for 30 min, followed by 4.5 h at 17 W/gel.

Preparative gels using the pool of all samples were run. For the IEF on a 24 cm pH 3–10 NL IPG strip, $900\,\mu g$ of protein sample was focused with the following program: $250\,V$ for $350\,V$ h, $500\,V$ for $600\,V$ h, $500-1000\,V$ for $900\,V$ h, $1000-4500\,V$ for $6500\,V$ h, $4500-8000\,V$ for $7000\,V$ h, $8000\,V$ for $42,200\,V$ h, and $500\,V$ for $1\,h$.

2.4. Image acquisition and 2D-DIGE data analysis

Gels were scanned in a Typhoon FLA 9500 biomolecular imager (GE Healthcare, USA) with filters for each fluorophore: Cy2 (488/520 nm), Cy3 (532/580 nm) and Cy5 (633/670 nm), set to $100\,\mu m$ resolution. Image cropping and multi-channel merging were carried out on using ImageQuant TL 7.0 software (GE Healthcare, USA). The Differential in Gel Analysis module of the DeCyder 2D 7.2 (GE Healthcare, USA) was used for automatic spot detection and abundance measurement in each signal-channel gel, by comparing the normalized volume ratio of each spot from a Cy3- or Cy5-labeled sample to their corresponding Cy2 signal from the internal standard. Differential in Gel Analysis was conducted on all the signal-channel gels and data sets collectively analyzed using the Biological Variation Analysis module (DeCyder 2D 7.2), which allowed inter-gel matching and calculation of a standardized average volume ratio (AVR) for each protein spot among all the gels. This was achieved firstly by identifying a master gel with the largest number of spots among all the internal standard gels (labeled by Cy2). Statistical analysis was conducted for each change in AVR using one-way ANOVA (statistical significance set at p value < .05), along with corresponding post-hoc analysis. Those protein spots from different groups with \pm 1.2-fold change in the AVR and with a p value < .05 were considered significantly differentially expressed.

Data was analyzed using principal components analysis and hierarchical cluster analysis (Distance metrics: Pearson Correlation; Linkage method: Complete Linkage) in the Extended Data Analysis module of DeCyder 2D 7.2; both analyses included all the protein spots with > 85% presence among all the gels and the set of spots with significant difference among the four groups.

2.5. Protein identification

Spots showing significant changes in protein abundance among groups were manually excised from the gel, washed in double-distilled water, then processed as follows. Spots were de-stained with $50\,\mu L$ of $30\,mM$ $K_3Fe(CN)_6;100\,mM$ $Na_2S_2O_3=1:1$ (v:v), and digested with $50\,ng$ of sequencing-grade trypsin (Promega, USA) overnight at $37\,^{\circ}C.$ After vacuum centrifugation peptides were resuspending in $2\,\mu L$ 20% ACN, and $1\,\mu L$ of peptide mixture was spotted onto a MALDI target plate and allowed to air dry at room temperature before adding $0.5\,\mu L$ of matrix, a supersaturated solution of α -cyano-4-hydroxy-transcinnamic acid (Sigma, USA) in 50% ACN/0.1% TFA; which was then left to air dry.

A 5800 MALDI-TOF/TOF mass spectrometer (Applied Biosystems, Canada) was operated in the positive reflector mode with an accelerating voltage of 2 kV. The scanning range was between 800 and 4000 Da. Eight of the most intense precursors with a minimum signal-to-noise of 50 were selected from each position. The CID-MS/MS spectra were acquired using a collision energy of 2 kV.

Database searching against both the NCBI nr database as well as a database created by six-frame translation of our antler stem cell transcriptome database [25], was performed using Mascot v2.2 (www. matrixscience.com). The database searching parameters were as follows: trypsin specificity; carbamidomethyl cysteine as a fixed modification and oxidized methionine as a variable modification; peptide mass tolerance: \pm 100 ppm; fragment mass tolerance: \pm 0.4 Da; 1 missed trypsin cleavage site; and the peptide charge state: 1+. Identifications were accepted as positive when a protein score C.I.% > 95% and at least one matching peptide with an ion score C.I.% > 95%.

2.6. Bioinformatics analysis

PANTHER v10.0 (http://www.pantherdb.org) was employed to perform functional classifications and enrichment analyses of Gene Ontology based on "biological process", "molecular function", and "protein class", on the DRPs between different groups [26].

Pathway network groups of the up- and down-regulated proteins were enriched and visualized by ClueGO v2.3.2 and CluePedia v1.3.2 plugins in Cytoscape v3.4.0 [27–29]. The Kappa score was used in ClueGO, as described by Huang et al. [30] to connect the pathway terms in the network. In the presentation of the data, node shapes represented the pathway database, i.e. diamond, ellipse, and hexagon were from the KEGG database, REACTOME database, and Wikipathways database, respectively. The main criteria were used as follows: the p value for each pathway term was calculated after a Bonferroni step down correction and only terms with p value < .05 were selected; the network specificity was set to medium; the kappa score, which was calculated based on the number of proteins shared between pathway terms, was set to 0.4; the leading group term was the one with the highest significance, and the group was named after it.

2.7. Validation by western blot

Proteins (35 µg) from each of the groups (n=3 samples/group), were loaded into the lanes of 5% stacking and 12% resolving SDS-PAGE gels and electrophoresed in Tris-Glycine-SDS buffer (Beyotime Biotechnology, China) at 200 mA for 45 min. Proteins on the SDS-PAGE gels were transferred to polyvinylidene fluoride (PVDF) membranes (0.45 µm; Merck Millipore, USA) in transfer buffer (25 mM Tris, 192 mM glycine and 20% (v/v) methanol). Membranes were then blocked for 2 h at room temperature with 5% skimmed milk in trisbuffered saline buffer containing 0.1% of Tween-20 (TBST; Bio-Rad, USA). Immunolabeling was conducted for 2 h at room temperature in TSBT with the following antibodies: rabbit polyclonal anti-HSP90AB1 (0.13 µg/mL; 11405-1-AP, Proteintech, China), rabbit polyclonal anti-HSPA5 (0.57 µg/mL; 11587-1-AP, Proteintech, China), rabbit

polyclonal anti-HNRNPK (0.25 μg/mL; 11426-1-AP, Proteintech, China), rabbit polyclonal anti-vimentin (0.27 µg/mL; 10366-1-AP, Proteintech, China), rabbit polyclonal anti-LGALS1 (1.00 µg/mL; YT1836, ImmunoWay, USA), rabbit polyclonal anti-SPARC (0.24 µg/ mL; 15274-1-AP, Proteintech, China) and mouse monoclonal anti-GAPDH (1:500-1:1000; AB-M-M001, Goodhere, China). After washing, the PVDF membranes were probed with goat anti-rabbit-HRP (1:2000; A0208, Beyotime Biotechnology, China) and goat anti-mouse-HRP (1:2000; A0216, Beyotime Biotechnology, China), separately for 1 h at room temperature. Blots were developed using an ECL Western Blotting Substrate Kit (Pierce Biotechnology, USA) following the manufacturer's manual, and images were taken on a Mini Chemi 610 Plus imaging system (SAGECREATION, China). The bands on each image were analyzed and quantified with ImageJ (National Institutes of Health, USA). Statistical analysis of band intensities was evaluated using Student's ttest in GraphPad Prism v7.0 (GraphPad Software, USA).

3. Results

3.1. Analysis of protein expression profiles by DeCyder

2D-DIGE proteomic analysis was performed on cell extracts from 12 biological samples (Table 1), corresponding to 4 experimental groups (n=3 per group) referred to as: FPCs, APCs, DPPCs and PPPCs. A technical repeat was also performed using the 12 biological replicates, with different pairing of the samples (Table 1). A representative image of the protein spots from a 2D-DIGE gel is shown in Fig. 2. 2D-DIGE images were subjected to computational analysis using DeCyder software and both multivariate and univariate analyses were applied to identify the similarity in protein expression profiles among experimental groups and the differences in protein abundance between each of the groups.

The inter-gel spot matching in the two repeated experiments revealed a total of 1278 and 1157 well defined spots, with 85% of the proteins present in at least 5 of the 6 gels. The average abundance of each spot among the 18 images was calculated and significant differences were considered when the p value < .05, both in one-way ANOVA as well as in the post-hoc analysis. The 2D-DIGE analysis is outlined in Fig. 3.

3.2. Multivariate statistics: principal component and hierarchical cluster analyses

Multivariate statistics allowed an evaluation of the whole data set, thus conferring a biological interpretation of the results, which was based on the integral protein expression profile of samples. Principal components analysis and hierarchical clustering analysis (Pearson correlation) were carried out on 284 (Fig. 4) and 164 (Fig. 5) validated

 $\begin{tabular}{ll} \textbf{Table 1} \\ \textbf{Experimental design of the first and second (technical replicate) experiments} \\ \textbf{for the CyDye labeling and sample combination in each of the 12 gels in the 2D-DIGE experiment. Each sample (1 to 3) is a biological replicate.} \\ \end{tabular}$

GEL N°	Cy2	Experiment 1		Experiment 2	
		СуЗ	Cy5	СуЗ	Cy5
1	IS	F1	P1	A2	D2
2	IS	A1	D1	F3	Р3
3	IS	F2	P2	A3	D3
4	IS	D2	A2	D1	F1
5	IS	D3	F3	P1	A1
6	IS	Р3	A3	P2	F2

IS: Internal Standard (pooled of all the samples); A: Antlerogenic periosteum stem cells (APCs); F: Facial periosteum cells (FPCs); D: Dormant pedicle periosteum stem cells (DPPCs); P: Potentiated pedicle periosteum stem cells (PPPCs).

spots and these revealed significant differences among groups (p value < .05 by one-way ANOVA). In both the initial and repeat experiment, the analyses identified three differentiated groups: the biological replicates from the FPCs (n=3), the biological repeats from the APCs (n=3) and the DPPCs and PPPCs samples (n=6) which were derived from pedicle periosteum and grouped together.

3.3. One-way ANOVA and post-hoc analysis

A total of 284 (first experiment) and 164 (second experiment for validation) differential spots were found, all of them displaying p value < .05 by one-way ANOVA (Fig. 3). The first experiments results were used for all subsequent analyses. To ensure accurate comparison of spots among gels, the correspondence of the 284 spots were manually validated through all the gels, and 92 spots were unambiguously confirmed and accurately identified by MS and database search (Fig. 3). Details of the computational comparison of differential spots between different groups are compiled in Table S1.

3.4. Identified DRPs

The 92 successfully identified spots corresponded to 63 DRPs. In a comparison of the PPPCs vs. DPPCs, the post-hoc analysis showed that there was only one spot (spot No. 1235, p value = .0224) with a significant difference. However, the average ratio of this spot was only 1.13, and thus did not reach the threshold value of \pm 1.2 set in this study (Table S1). Comparison of the APCs vs. FPCs found 23 DRPs, of which 7 were up-regulated and 16 down-regulated in the APCs (Fig. 6 and Table S2). The PPC where considered as one group however differences of PPPCs and DPPCs to FPCs were analyzed. There were 24 DRPs for both PPPCs and DPPCs compared to the FPCs and of these 12 were up-regulated and 12 down-regulated. In addition, 4 up-regulated and 4 down-regulated proteins were only found in the PPPCs vs. FPCs; and 8 up-regulated and 4 down-regulated proteins found in the DPPCs vs. FPCs only (Fig. 7 and Table S3).

The highest number of DRPs were detected when comparing the PPCs (PPPCs and DPPCs) to the APCs. A total of 61 proteins were significantly up- or down- regulated (34 and 27, respectively) in both the PPPCs and DPPCs groups compared to the APCs. In addition, 8 upregulated and 6 down-regulated proteins were detected in the PPPCs vs. APCs alone and 9 up-regulated and 1 down-regulated protein detected in the comparison of DPPCs vs. APCs alone (Fig. 8 and Table S4).

3.5. Functional classification of the DRPs

PANTHER 10.0 bioinformatics software was used to categorize the Gene Ontology of all the DRPs in biological process, molecular function and protein class (Fig. 9). The DRPs in the three comparisons (APCs vs. FPCs, PPCs vs. FPCs, PPCs vs. APCs) were all mapped. The PPCs vs APCs comparison, which contained the largest number of DRPs, also gave the largest number of classifications.

Within the classification of 'biological process', the DRPs were mainly (70% of the total processes) involved in "cellular process", "metabolic process" and "cellular component organization or biogenesis", successively. In the APCs vs. FPCs comparison there were no proteins involved in "response to stimulus" and "immune system process"

As to the classification based on molecular function, the majority of DRPs possessed "catalytic activity", "structural molecule activity" and "binding function" in all the three comparisons; although the order in the APCs vs. FPCs was different. Regarding other categories, there were no DRPs with "antioxidant activity" or "channel regulator activity" found in the APCs vs. FPCs, and no "translation regulator activity" or "channel regulator activity" found in the PPCs vs. FPCs.

Classification based on protein class resulted in the identification of five major categories in the PPCs vs FPCs and PPCs vs APCs:

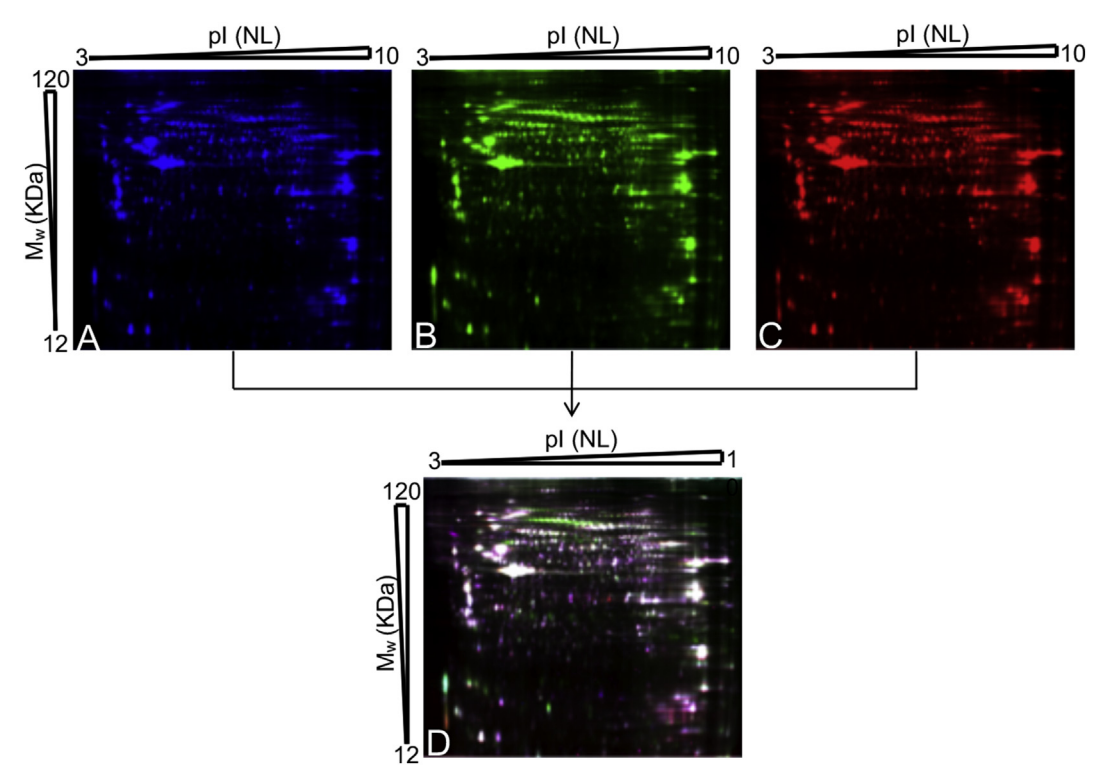


Fig. 2. Representative 2D-DIGE images of protein profiles (Gel 3 in experiment 1; Table 1). In these images the protein samples of facial periosteum cells (FPCs), potentiated pedicle periosteum cells (PPPCs) and the internal standard (IS) were individually labeled with fluorescent dyes, mixed together and separated by 2D-DIGE followed by Typhoon image scanning. (A) IS made of pooled proteins from all samples labeled with Cy2 dye (Master gel); (B) Image of the FPC labeled with Cy3 dye; (C) Image of the PPPC labeled with Cy5 dye; and (D) Overlay gel of the FPC, PPPC and the IS.

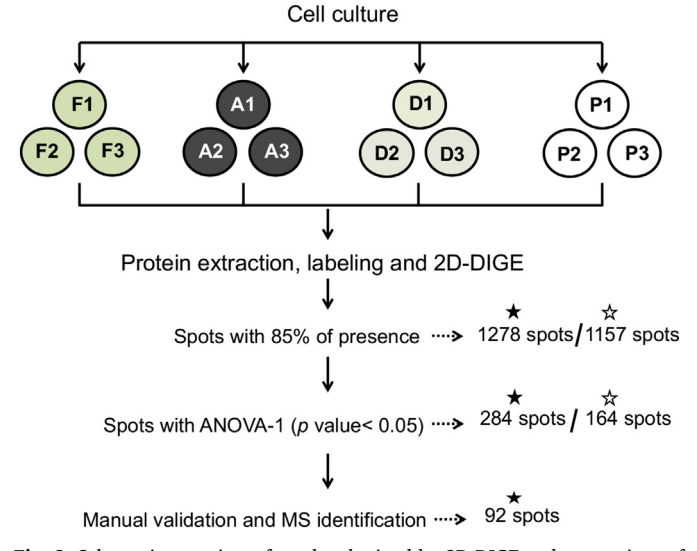


Fig. 3. Schematic overview of results obtained by 2D-DIGE and comparison of the protein profiles of cells isolated from the facial periosteum (F), antlerogenic periosteum (A), dormant pedicle periosteum (D) and potentiated pedicle periosteum (P). Black star: experiment 1; white star: experiment 2.

"cytoskeletal protein", "chaperone", "hydrolase", "enzyme modulator" and "oxidoreductase" successively. In the APCs vs FPCs comparison, the top five categories were "cytoskeletal protein", "enzyme modulator", "nucleic acid binding", "transporter" and "hydrolase". The PPCs vs APCs comparison was unique in that it contained proteins that mapped to "cell adhesion molecule" and "extracellular matrix protein" but not to "transfer/carrier protein".

3.6. Enriched pathways network analysis of the DRPs

The pathway network groups that mapped with the DRPs were enriched using the ClueGo plugin. The enrichment network of the DRPs with their expression level in each pathway (p value \leq .05) was then created using the CluePedia plugin from the Cytoscape platform. In the APCs vs. FPCs (Fig. 10), there were two groups and three independent pathways. In the "recycling pathway of L1" and "vasopressin-regulated water reabsorption", all the enriched proteins were down-regulated in the APCs. In the pathway groups – "smooth muscle contraction" and "leukocyte transendothelial migration", the majority of enriched proteins were down-regulated in the APCs. Only in the "prostaglandin synthesis and regulation pathway", were the enriched DRPs (75%) found up-regulated in the APCs.

In the comparison of PPCs vs. FPCs, there were three enriched pathway network groups (Fig. 11 and S1), which were "cooperation of PDCL (PhLP1) and TRiC/CCT in G-protein beta folding", "smooth muscle contraction" and "leukocyte transendothelial migration". Nearly all the enriched pathways had more up-regulated proteins in the PPCs. An exception to this was in the pathway "the role of GTSE1 in G2/M progression after G2 checkpoint", where 75% of the enriched proteins were down-regulated in the PPCs.

The enriched pathway network groups in the PPCs vs. APCs comparison (Fig. 12 and S2) were mainly "chaperonin-mediated protein folding", "smooth muscle contraction", "parkin-ubiquitin proteasomal system pathway" and "cooperation of prefoldin and TriC/CCT in actin and tubulin folding". Among them, there were more up-regulated proteins found in the PPCs from the first three groups but less in the fourth group.

3.7. Western blot validation of the selected DRPs

The differences in abundance of DRPs from the four samples were

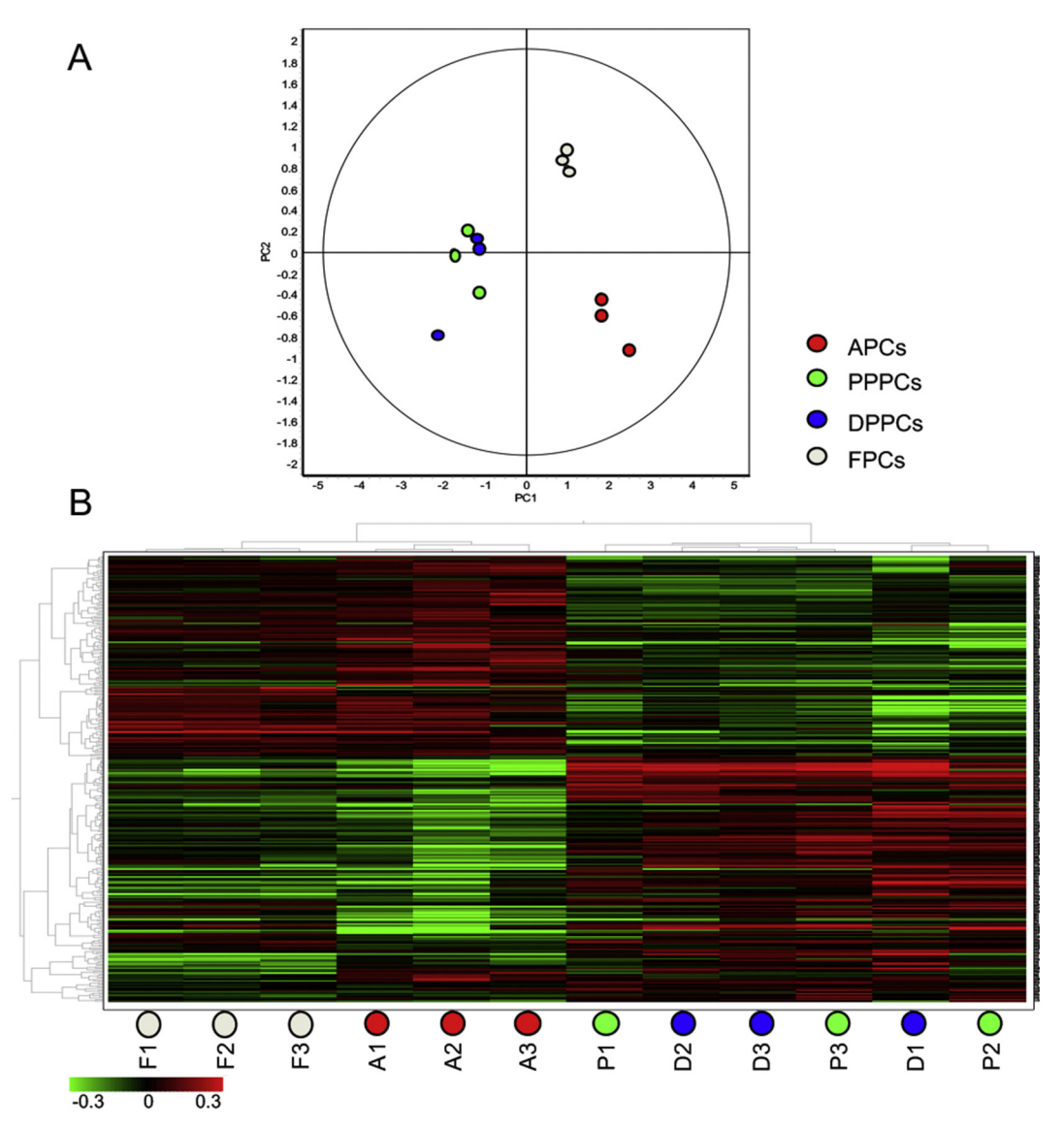


Fig. 4. Multivariate statistical analysis applied to the 284 differential spots obtained in the first 2D-DIGE experiment (ANOVA-1; p value < .05). (A) Two-dimensional score plot from the principal components analysis of the 12 biological replicates. (B) Heat-map with dendrograms from the hierarchical clustering analysis (Pearson correlation). Rows represent individual proteins and columns are the biological replicates (n = 3) as indicated at the bottom of the graph: facial periosteum cells (F), antlerogenic periosteum cells (A), dormant pedicle periosteum cells (D) and potentiated pedicle periosteum cells (P). The colour in each block represents the protein expression level, using a standardized log abundance scale ranging from negative (green) to positive (red) values. (For interpretation of the references to colour in this figure legend, the reader is referred to the web version of this article.)

validated by western blot (Fig. 13). Glyceraldehyde-3-phosphate dehydrogenase (GAPDH) was used to normalize loading of the selected proteins. Consistent with the 2D-DIGE results no significant differences were detected between PPPC and DPPC groups. In the comparisons for PPCs vs. FPCs and PPCs vs. APCs, all the results with significant difference in western blot had the same trend of expression level as their corresponding 2D-DIGE results. HSPA5 in the 2D-DIGE results had three spots with different expression trends in the comparison of DPPCs vs. FPCs, making interpretation of the results difficult. Vimentin was a slight exception as it had similar levels in the APCs and FPCs by western blot analysis but was slightly up-regulated in the APCs when examined by 2D-DIGE; however, the elevated levels in the AP and FP over PPP and DPP were consistent. Overall, the relative expression levels of the selected proteins between 2D-DIGE and western blot were found to be consistent.

4. Discussions

Understanding the regulation of stem cells and how these pools of multipotent cells are controlled is of importance in the field of regenerative biology. This study examined the different protein expression profiles of APCs and PPCs and compared them to FPCs as controls. The aim was to use the antler as a model to discover protein targets associated with maintenance and activation of stem cells and examine the protein networks and possible molecular mechanisms involved in regulating tissue/organ generation and regeneration.

4.1. Multivariate statistical analysis

The hierarchical cluster analysis (Figs. 4B and 5B), showed good overall agreement with the principal component analysis (Figs. 4A and 5A). Protein expression profiles were found to be different between the APCs and FPCs, while the DPPCs and PPPCs were very similar (Figs. 4 and 5). FPCs and APCs are both derived from the periosteum over the

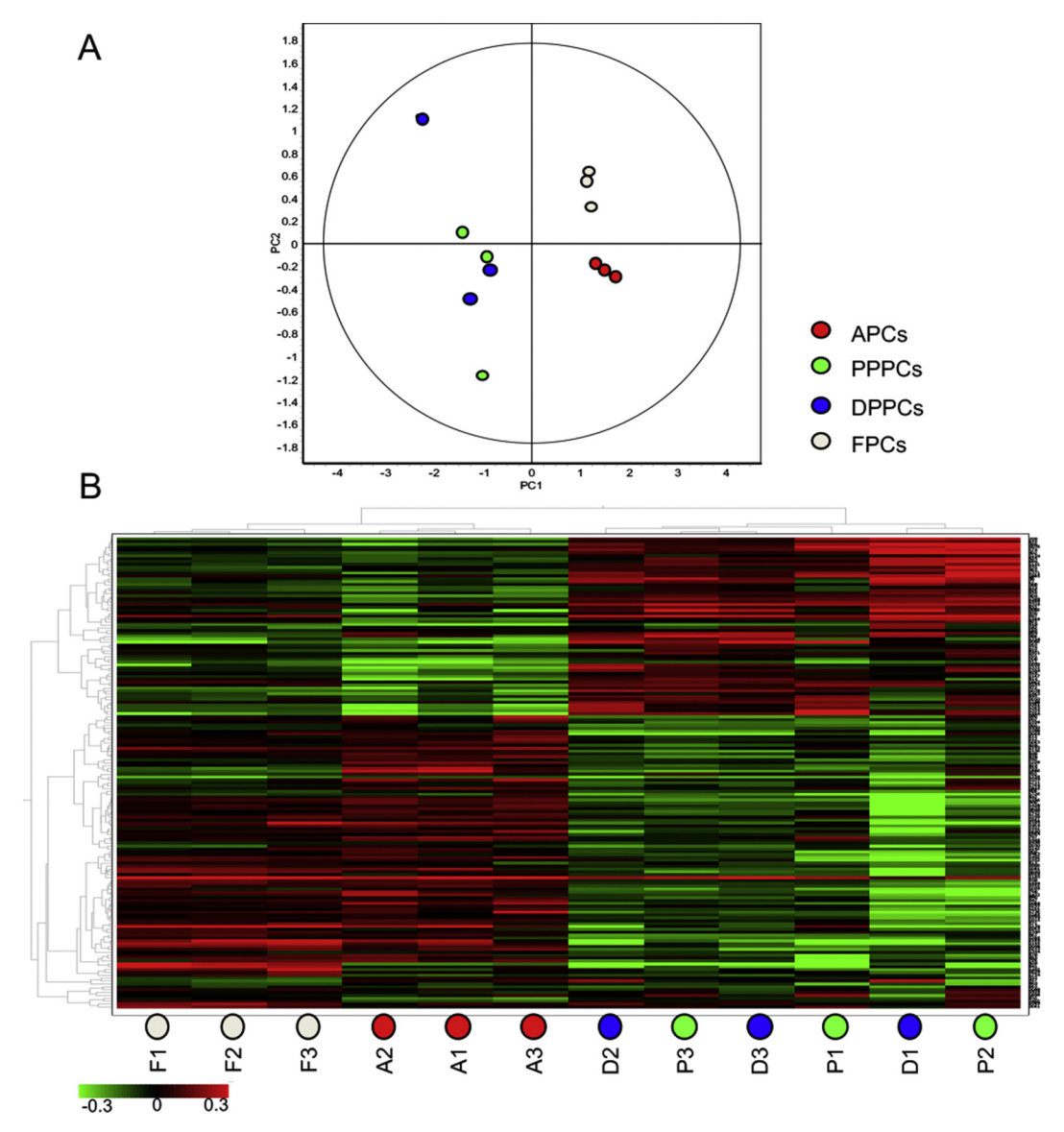


Fig. 5. Multivariate statistical analysis applied to the 164 differential spots obtained from the second 2D-DIGE experiment (ANOVA-1; *p* value < .05). (A) Two-dimensional score plot from the principal components analysis of the 12 biological replicates. (B) Heat-map with dendrograms from the hierarchical clustering analysis (Pearson correlation). Rows represent individual proteins and columns are the biological replicates (n = 3) as indicated at the bottom of the graph: facial periosteum cells (F), antlerogenic periosteum cells (A), dormant pedicle periosteum cells (D) and potentiated pedicle periosteum cells (P). The colour in each block represents the protein expression level, using a standardized log abundance scale ranging from negative (green) to positive (red) values. (For interpretation of the references to colour in this figure legend, the reader is referred to the web version of this article.)

cervine skull [11], in the vicinity geographically, and in the hierarchical cluster analysis they were most similar. The pedicle periosteum cells from the dormant (DPPCs; proximal two thirds) and potentiated regions (PPPCs; distal third) [31] clustered together, and in the subsequent analyses were considered as one group. The lack of difference between these stem cell groups suggests that the stem cell activation zone, responsible for the production of new antler at the most distal aspect of the pedicle, may be smaller than previously thought; alternatively, 2D-DIGE method may not be sensitive enough to detect the low abundant proteins that might involve in this activation.

4.2. DRPs and antler generation

The FPCs were collected from over intramembranous bone and are known to contain resident mesenchymal stem cells capable of bone repair and regeneration [32,33]. The AP is located in a unique region where the stem cells are capable of generating antler in the first year.

There were more down-regulated proteins in the APCs when compared to the control FPCs (Fig. 6), which was consistent with the findings in the pathway groups (Fig. 10). These results may mean that AP tissue at the time of sampling was still metabolically quiescent.

The majority of the APCs down-regulated proteins was mapped to the categories of "structural molecule activity" (39%) and "cytoskeletal protein" (39%; Fig. 9) and consisted of: actin cytoplasmic 1 (ACTB); moesin (MSN); actin aortic smooth muscle (ACTA2); alpha-actinin-4 (ACTN4). Normally, the cytoskeletal proteins function by regulating cellular proliferation [34], migration and motility [35,36]. This may indicate that, in the present experiment, the APCs had less cellular motility compared with the FPCs. At the time of collection, the specialized antler stem cells of the AP were in dormant and thus the presence of multiple down-regulated proteins was consistent with the biological status of the tissue.

Prostaglandins are a group of active lipid signaling molecules, which are widely distributed in a large number of tissue types. They

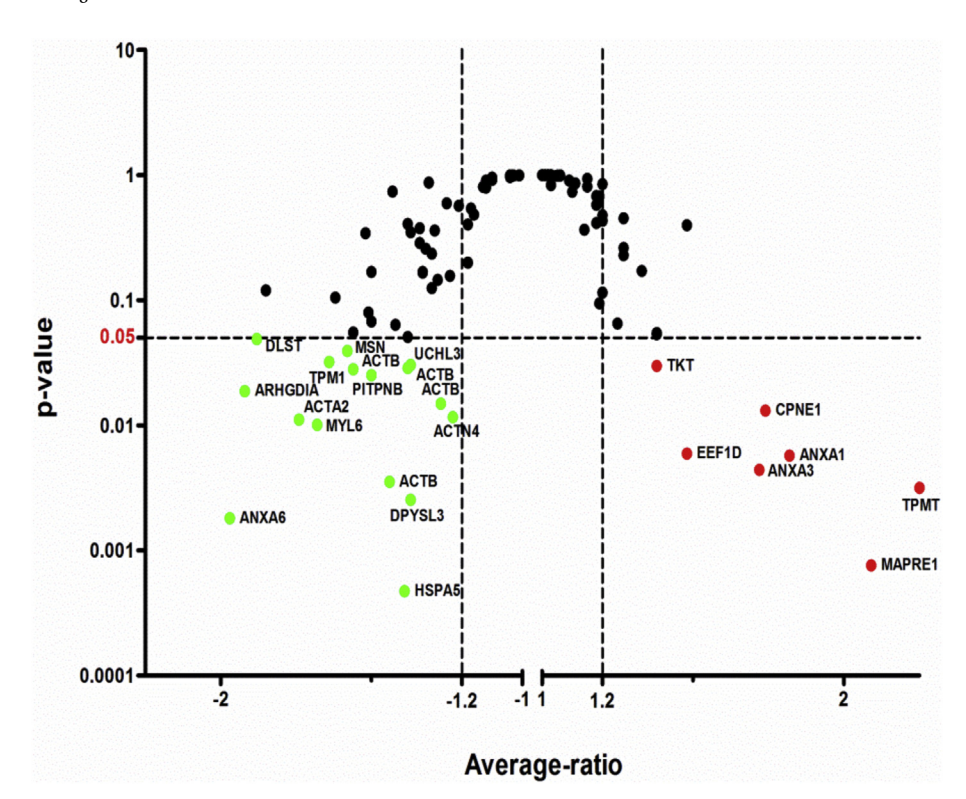


Fig. 6. Differentially expressed proteins in the antlerogenic periosteum cells (APCs) as compared to the facial periosteum cells (FPCs). Y axis denotes the p value with p=0.05 marked by a dotted line. X axis represents the up and down regulated proteins in the APCs vs FPCs where \pm 1.2 fold regulation values are marked by lines. Red = up-regulated proteins > 1.2 and p value < .05; green = down-regulated proteins of the references to colour in this figure legend, the reader is referred to the web version of this article.)

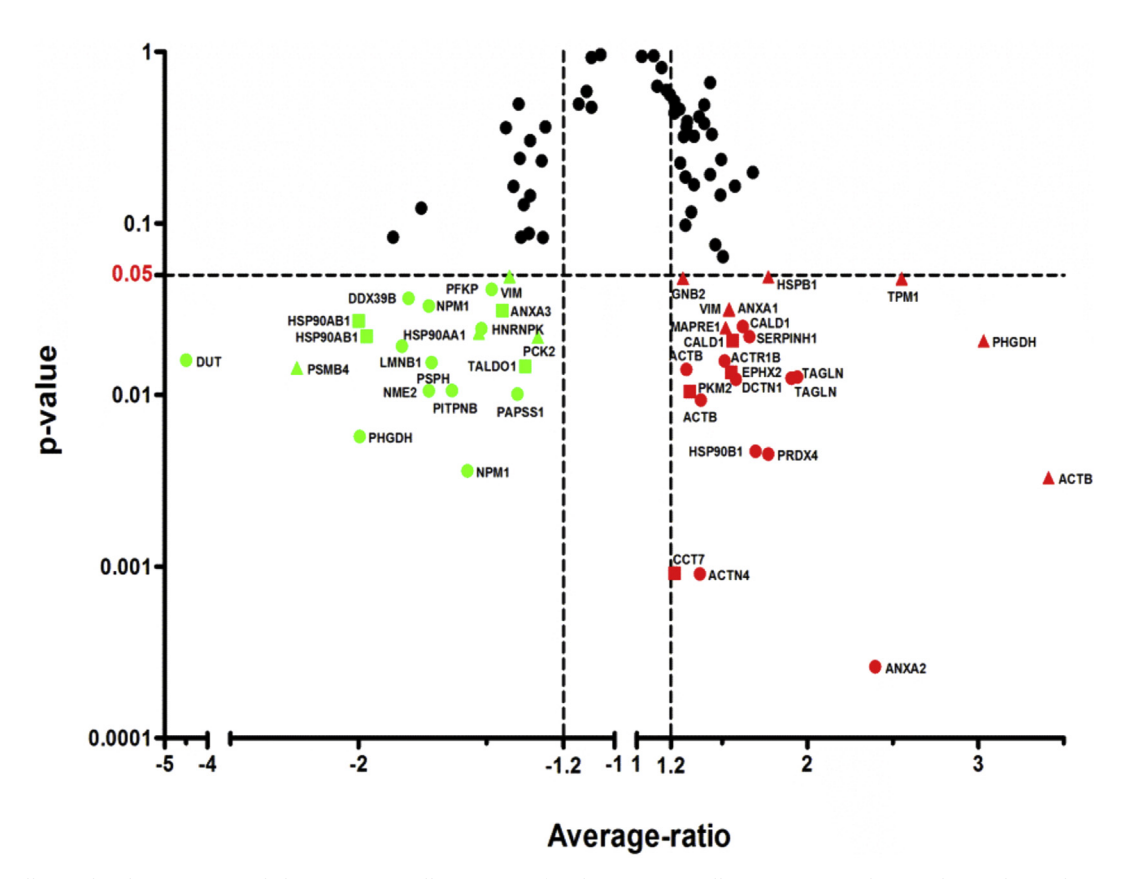


Fig. 7. Differentially regulated proteins in pedicle periosteum cells (PPCs) vs. facial periosteum cells (FPCs). Y axis denotes the p value with p=.05 marked by a dotted line. X axis represents the up and down regulated proteins in the PPCs vs FPCs where \pm 1.2 fold regulation values are marked by lines. Red = up-regulated proteins > 1.2 and p value < .05; green = down-regulated proteins < -1.2 and p value < .05. Circular dots mean proteins were significantly different in both the potentiated and dormant PPCs when compared to the FPCs; rectangular dots = only significantly different in the potentiated PPCs vs. FPCs; and triangular dots = only significantly different in the figure legend, the reader is referred to the web version of this article.)

Journal of Proteomics 195 (2019) 98-113

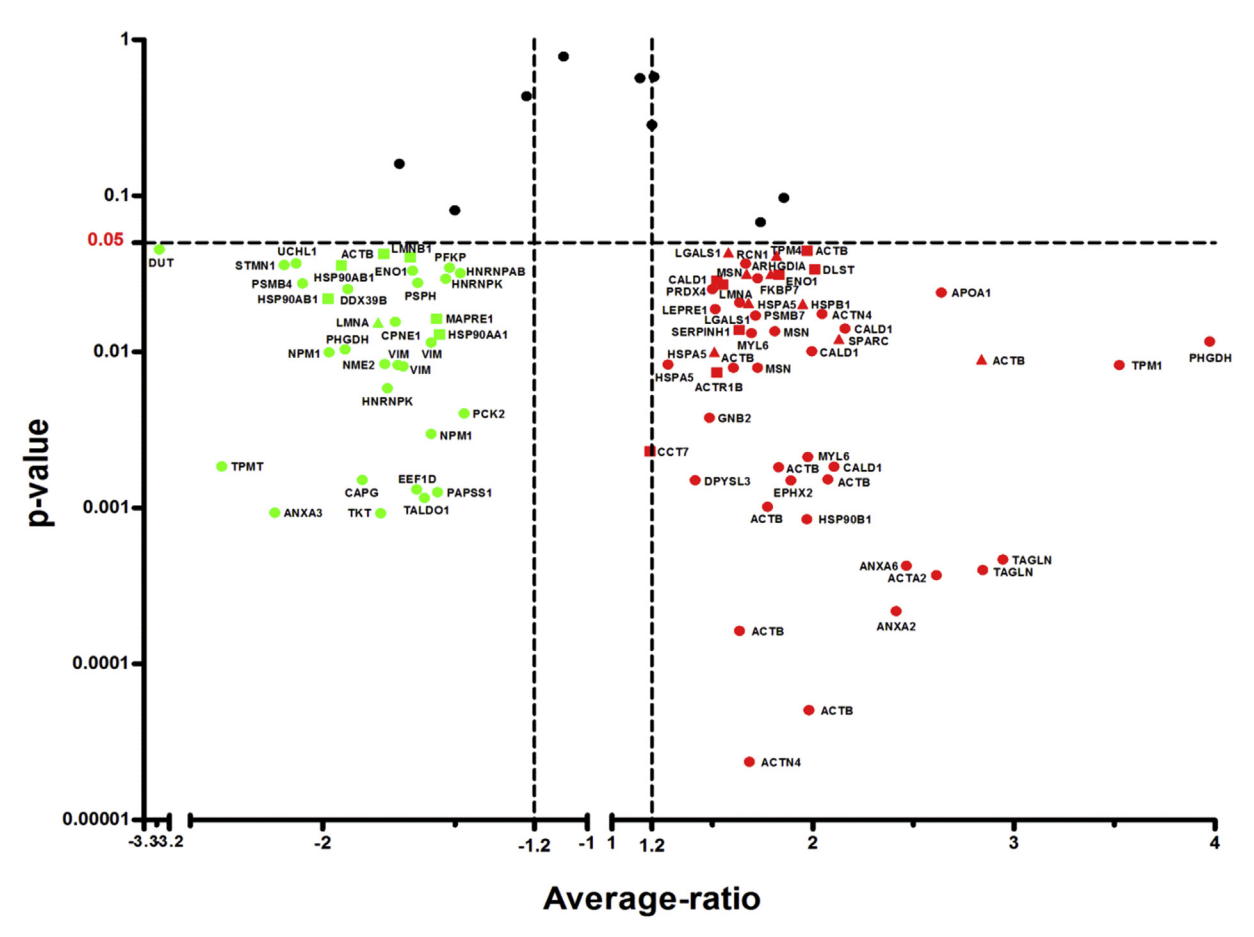


Fig. 8. Differentially regulated proteins in the pedicle periosteum cells (PPCs) vs. antlerogenic periosteum cells (APCs). Y axis denotes the p value with p=0.05 marked by a dotted line. X axis represents the up and down regulated proteins in the PPCs vs APCs where \pm 1.2 fold regulation values are marked by lines. Red = upregulated proteins > 1.2 and p value < .05; green = down-regulated proteins < -1.2 and p value < .05. Circular dots mean proteins were significantly different in both the potentiated and dormant PPCs when compared to the APCs; rectangular dots = only significantly different in the potentiated PPCs vs. APCs; and triangular dots = only significantly different in the dormant PPCs vs. APCs. (For interpretation of the references to colour in this figure legend, the reader is referred to the web version of this article.)

have multiple biological activities, such as promotion of inflammation [37], apoptosis and angiogenesis [38]. Prostaglandins have also been associated with the regeneration processes in many kinds of tissues including: skin [39], muscle [40], cartilage [41], bone marrow, liver and colon [42]. The only enriched molecular pathway with more upregulated proteins for the APCs was "prostaglandin synthesis and regulation" which suggests prostaglandins may play a role in the maintenance of the stemness for APCs.

4.3. PPCs responsible for antler regeneration

The PPCs which are responsible for driving annual antler regeneration were also compared to the FPCs. More DRPs were found to be up-regulated in the PPCs vs FPCs (Fig. 7) than when the APCs were compared to the FPCs (Fig. 6). Cytoskeletal proteins (29% from the protein class; Fig. 9) and nearly all the enriched pathway groups (Fig. 11), were now largely up-regulated in the PPCs vs FPCs comparison.

Multiple pathways which contain proteins GNB1, GNB2, GNG4, and CCT7 were enriched in the pathway group "cooperation of PDCL (PhLP1) and TRiC/CCT in G-protein beta folding" (Fig. S1). In humans, there are 616 identified G protein-coupled receptors (GPCRs) [43], which transduce signals to intracellular heterotrimeric G proteins which are then catalytically activated [44] to mediate the downstream effectors from multiple ligands, such as neurotransmitters, hormones, metabolites, and sensory signals [45]. Some GPCRs are found to play

very important roles in regenerative medicine, such as in nerve repair, bone healing and formation, myocardial regeneration and newt limb regeneration [46–51]. These results suggest there were more well-assembled heterotrimeric G proteins and well-folded GPCRs in the stem cells from the PPCs than in the FP derived cells.

The only enriched pathway with more down-regulated proteins (75%) than up-regulated in the PPCs was "the role of GTSE1 in G2/M progression after G2 checkpoint" (Fig. 11). In this pathway, GTSE1 binds MAPRE1 to promote cell migration [52]. More MAPRE1 protein was found in the PPCs (Fig. 7), which would be consistent with the PPCs having a greater capability to migrate and produce new antler. Notable was the down-regulation of HSP90AA1 and HSP90AB1, the two cytosolic isoforms of HSP90 [53], in the PPCs as detected by both 2D-DIGE (Fig. 7) and western blotting (Fig. 13). Considering the multiple functions of HSP90 [54], this pathway warrants further investigation.

Within the Reactome pathway, GTSE1 binds p21 with the aid of FKBPL and chaperone protein HSP90 to form a stable quadruple cytosolic complex. This complex delays G2/M onset and rescues cells from G2 checkpoint-induced apoptosis [55]. In this research, the PPCs had higher expression of GTSE1 and p21 which may mean that when compared with the FPCs, cells were more likely to be in the G1 phase, a finding which was consistent with our previous work [56].

4.4. Protein expression profiles in different types of antler stem cells

There were more DRPs (Fig. 8), greater number of Gene Ontology

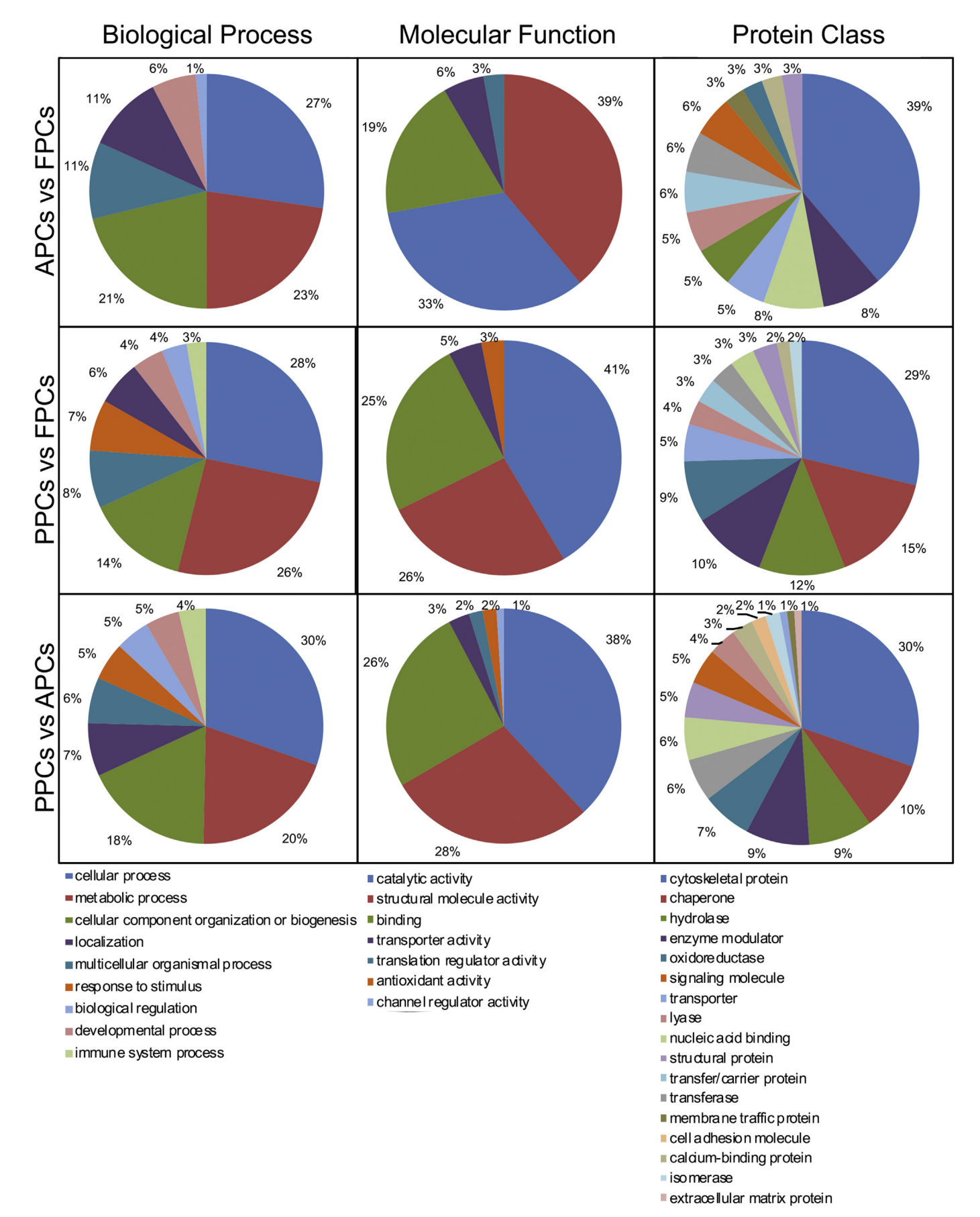


Fig. 9. Gene Ontology (GO) classification of the differentially expressed proteins using PANTHER 10.0. Percentages of GO terms in each category are displayed.

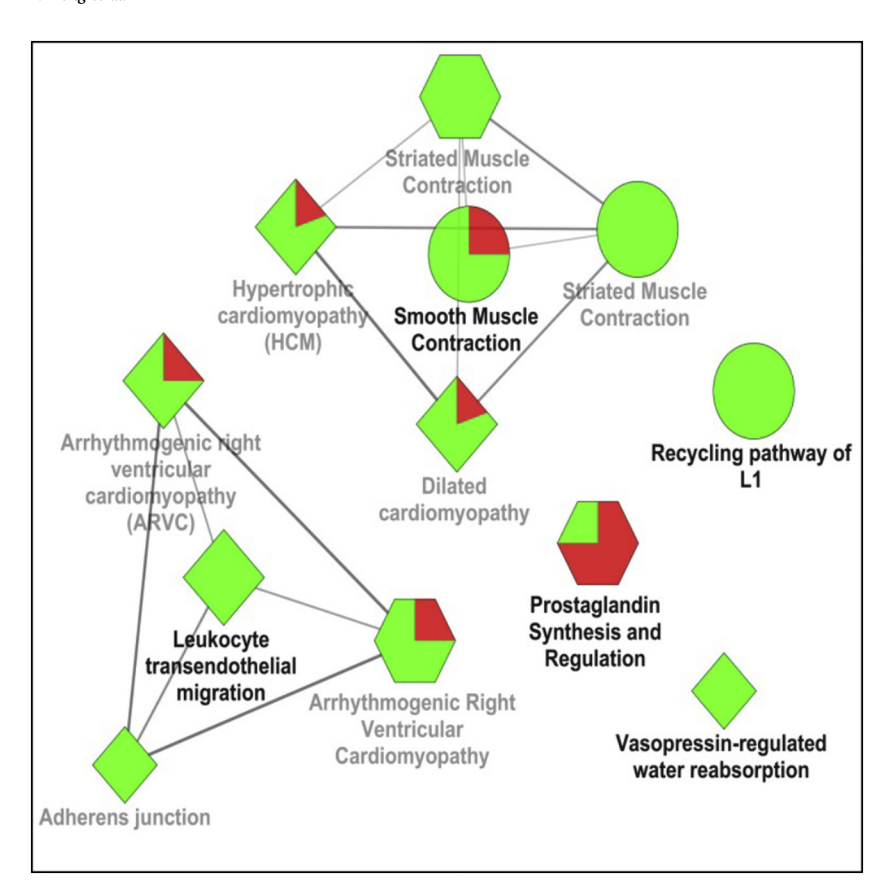


Fig. 10. Enriched pathway network groups for the differentially regulated proteins in the antlerogenic periosteum cells (APCs) vs. facial periosteum cells (FPCs) comparison. Pathways for the significantly up- and down-regulated proteins of the APCs are visualized as a functionally grouped network based on the kappa score (0.4); only the terms that have p value ≤.05 are shown. The size of the nodes denotes the term significance. The most significant term of each group is highlighted, and the group is named after it. Nodes in different shapes (diamond: KEGG database; ellipse: REACTOME database; hexagon: Wikipathways database) represent specific pathways and are grouped based on their similarity. The proportions of up- or down-regulated proteins in each pathway are indicated by red or green respectively. (For interpretation of the references to colour in this figure legend, the reader is referred to the web version of this article.)

classifications (Fig. 9) and more enriched pathways (Fig. 12) in the comparison of PPCs vs. APCs. Collectively, this may imply that compared to the APCs, the PPCs have unambiguously differentiated into another type of stem cells. Among the enriched pathway groups (Fig. 12), the group entitled "smooth muscle contraction" had more upregulated proteins. This "smooth muscle contraction" enrichment group was identified not only in the PPCs vs. APCs, but also from the other two comparisons conducted in this research. The up-regulated protein CALD1 is an actin- and myosin-binding protein working as a bridge between actin and myosin molecules in both muscle and in non-muscle cells [57,58], and important in stabilizing the cytoskeleton [59]. In the antler stem cells, CALD1 may have relations with actin filaments like ACTA2 and ACTN4, the myosin protein like MYL6 and TPM family (TPM1-4), and with the help of the Ca²⁺/calmodulin complex, function to stabilize the cytoskeleton and increase cell motility. These proteins, when detected, were up-regulated in the PPCs as compared to the APCs (Fig. S2). Another two enriched molecules found up-regulated in the PPCs were annexin A2 and A6 (Fig. S2). Annexins are a family of phospholipid-binding proteins which are controlled in a Ca²⁺-dependent manner [60]. ANXA2 and ANXA6 bind with dysferlin and have a role in the rapid resealing of disrupted cell membranes both in skeletal muscle and cardiomyocytes [61,62]. This implies ANXA2 and ANXA6 up-regulation in the PPCs may be involved in membrane repair and maintenance. PPCs provide the sole cell source for regenerating antlers [15], and these cells not only differentiate into bone lineage cells to build up antler tissue, but also may differentiate into cell types for building up blood vessels [63]. Antler blood vessels are unique in that they have unprecedented contract force when mechanically stretched [12]. Therefore, one possible reason is that up-regulation of smooth muscle contraction in the PPCs may have laid the foundation for the future construction of the unique blood vessels. In addition, upregulation of these enriched DRPs may also indicate that the antler stem cells had some muscle cell-like potential, such as executing aggressive and powerful cell motility. This finding is consistent with the ability of the

PP to regenerate antler on an annual basis.

Neural crest stem cells are unique to developing vertebrate embryos and can differentiate into multiple tissue types such as neurons, glia, craniofacial cartilage, bone, teeth and smooth muscle [64]. Antler stem cells have been conjectured to be derived from neural crest cells [9,65,66]. The PP cells have also been experimentally defined as persistent neural crest-like stem cells [67]. The epithelial-mesenchymal transition (EMT) process is well known to play a key role in the migration and differentiation of the neural crest [68,69]. The transcriptional master-regulator of EMT is the Slug protein [70] and has been found in higher levels in the PP during the regenerative phase compared to the non-regenerative phase [67], which suggests that EMT activation may be important for antler regeneration. In this research, SPARC, galectin-1 (Figs. 8 and 13) and S100A4 [71] were all found to be up-regulated in the PPCs comparing to the APCs. These proteins are all markers of EMT induction [72-78]. This supports a role for EMT activation in antler wound healing (the very initial stage of antler regeneration) and regeneration.

Less vimentin protein was detected by both 2D-DIGE and western blotting in the PPCs as compared to the APCs. Vimentin is a major cytoskeletal component and often used as a marker of mesenchymal-derived cells [79,80] or cells undergoing EMT [81]. The significance of vimentin reduction and its effects on cell mobility and deformability warrants further research in relation to the regulation of the PPCs.

The "pentose phosphate pathway" was one of few enriched pathways with all down-regulated proteins in the PPCs comparing to the APCs (Fig. 12). Together with PFKP from "glycolysis" and PCK2 from "gluconeogenesis" (Fig. 8 and S2), this may indicate that carbohydrate metabolism was more active in the APCs. These glucose metabolism pathways produce energy, such as ATP, and some products are important for cellular processes, like the NADPH and ribose 5-phosphate (R5P) from the pentose phosphate pathway [82]. The two enzymes, TKT and TALDO1, enriched in the "pentose phosphate pathway" (Fig. S2) were both involved in its non-oxidative phase [83].

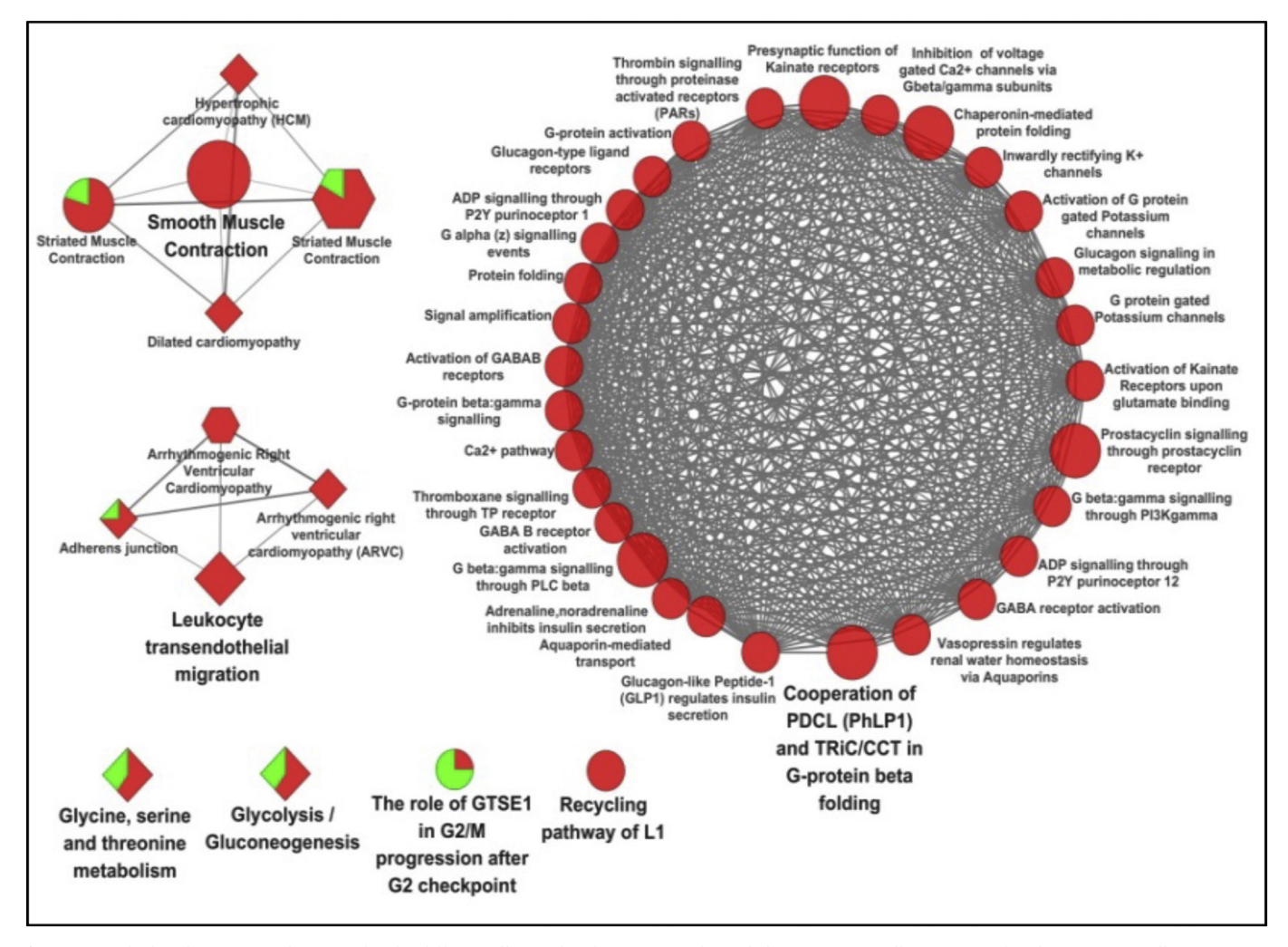


Fig. 11. Enriched pathway network groups for the differentially regulated proteins in the pedicle periosteum cells (PPCs) vs. facial periosteum cells (FPCs) comparison. Pathways for the identified up- and down-regulated proteins of the PPCs are visualized as a functionally grouped network based on the kappa score (0.4); only the terms that have p value ≤ .05 are shown. The size of the nodes shows the term significance. The most significant term of each group is highlighted, and the group is named after it. Nodes in different shapes (diamond: KEGG database; ellipse: REACTOME database; hexagon: Wikipathways database) represent specific pathways and are grouped based on their similarity. The proportions of up- or down-regulated proteins in each pathway are indicated by red or green respectively. (For interpretation of the references to colour in this figure legend, the reader is referred to the web version of this article.)

DUT protein had the lowest level in the PPCs compared to the APCs (AVR = -3.24; p value = .045). DUT is an enzyme which participates in nucleotide metabolism, regulating the production of dUMP from dUTP, and as such plays a critical role in the fidelity of genomic replication and repair [84]. In the APCs the DUT protein may create more R5P through the nucleotide salvage pathway. This would contribute to the stability of the genome and provide more substrate to the pentose phosphate pathway from unwanted dNTPs [85]. Interestingly, DUT was also highly up-regulated in the FPCs compared to the PPCs (Fig. 7). The underlying mechanism between the different expression levels of DUT is worthy of further investigation.

5. Conclusions

This is the first comprehensive study of the protein profiles from the antler stem cells involved in antler generation and regeneration using a quantitative protein-labeling technique (2D-DIGE). The analyses of the DRPs demonstrated that multiple cell processes and signaling pathways were involved in regulating the maintenance and activation of stem cells fundamental to the development of antler as a complex organ. The EMT process was identified as a key element in the PPCs and may contribute to the initial stage of antler regeneration, i.e. scar-less

healing and antler regeneration per se. This research points to the regulation of cytoskeletal proteins and particularly those involved in smooth muscle contraction being important in the PPCs, which are capable of antler regeneration and thus requiring high mobility. Energy metabolism within the PPCs may however be lower than that of the APCs or FPC. In addition, DUT is a potential marker to distinguish APCs/FPCs from PPCs. The antler provides an exciting model to investigate mammalian neural crest derived stem cells, proteins and process that control regenerative capacity.

Conflict of interest

The authors declare that they have no conflict of interest.

Acknowledgements

This work was supported by the Strategic Priority Research Program of the Chinese Academy of Sciences, Grant No XDA16010105 and National Natural Science Foundation of China, Grant No 31500792. We would like to thank Velvet Antler Research New Zealand (VARNZ) and the University of Otago for their assistance with funding for Zhen Dong. We acknowledge the supply of antler stem cells transcriptome database

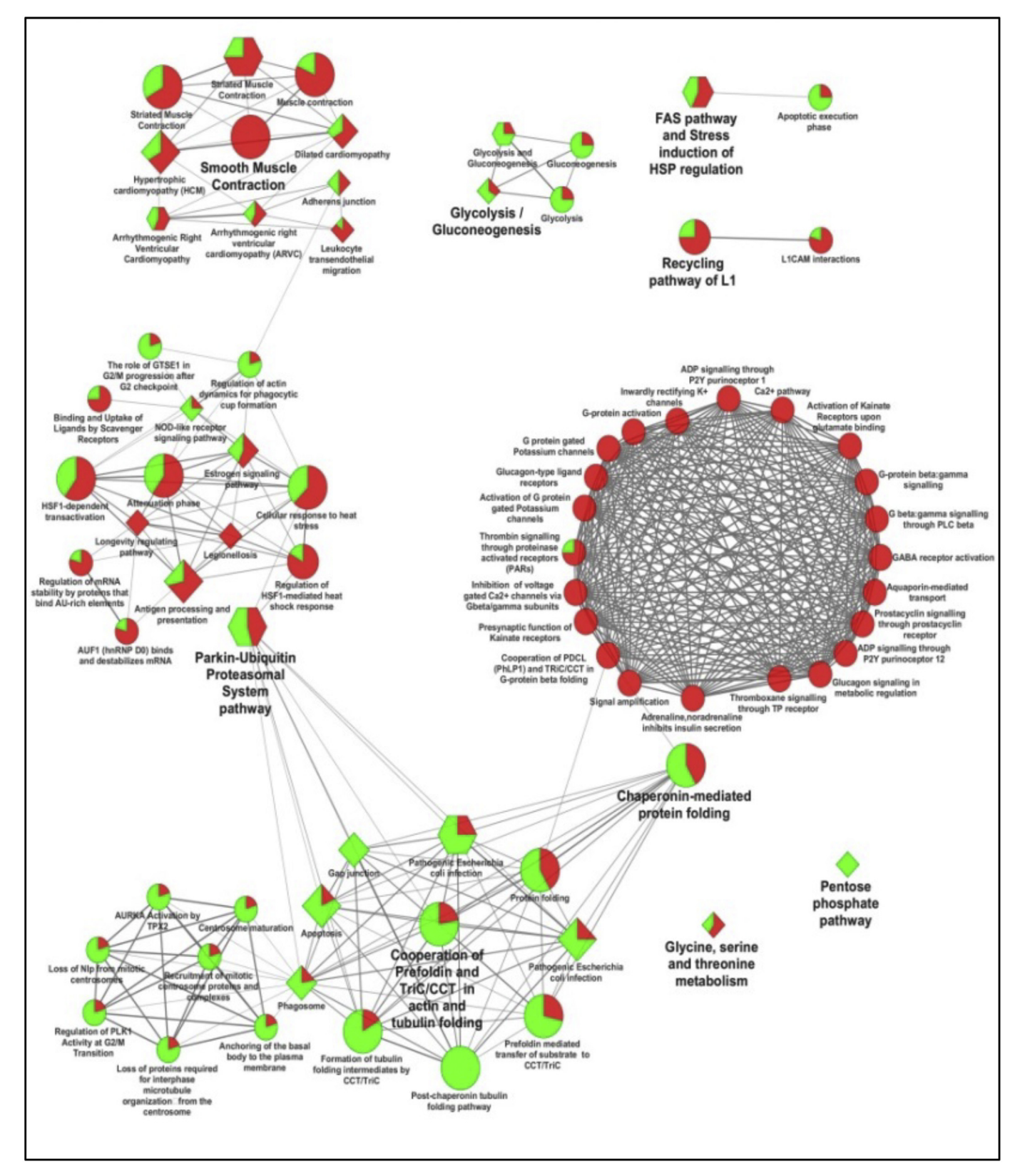


Fig. 12. Enriched pathway network groups for the differentially regulated proteins in the pedicle periosteum cells (PPCs) vs. antlerogenic periosteum cells (APCs) comparison. Pathways for the identified up- and down-regulated proteins of the PPCs are visualized as a functionally grouped network based on the kappa score (0.4); only the terms that have p value \leq .05 are shown. The size of the nodes shows the term significance. The most significant term of each group is highlighted, and the group is named after it. Nodes in different shapes (diamond: KEGG database; ellipse: REACTOME database; hexagon: Wikipathways database) represent specific pathways and are grouped based on their similarity. The proportions of up- or down-regulated proteins in each pathway are indicated by red or green respectively. (For interpretation of the references to colour in this figure legend, the reader is referred to the web version of this article.)

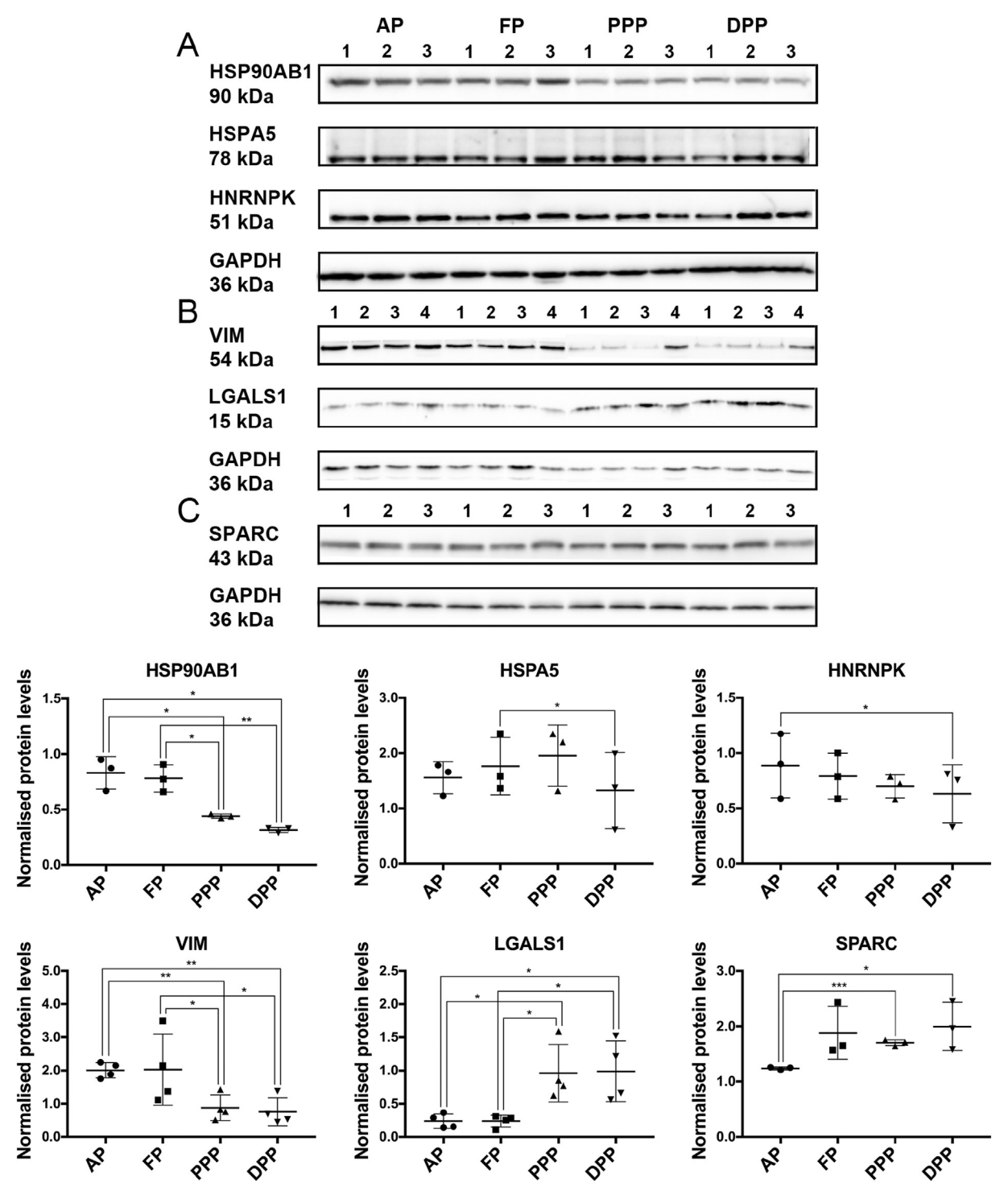


Fig. 13. Western blot analysis of the differentially regulated proteins in the four groups. The same amount of protein of each biological replicate employed in 2D-DIGE was detected with (A): anti-HSP90AB1, anti-HSPA5, anti-HNRNPK, (B): anti-VIM, anti-LGALS1, and (C): anti-SPARC. Anti-GAPDH was used as the endogenous control. Band intensities were quantified using Image J. AP: antlerogenic periosteum cells; FP: facial periosteum cells; PPP: potentiated pedicle periosteum cells. Protein abundance in each experimental group is expressed as the mean value \pm standard deviation in normalized protein levels. * p value < .01, *** p value < .001.

by Dr. Hengxing Ba from the Institute of Special Wild Economic Animals and Plants from the Chinese Academy of Agricultural Sciences, China. We thank Quanwei Wang for technical assistance.

Appendix A. Supplementary data

Supplementary data to this article can be found online at https://

doi.org/10.1016/j.jprot.2019.01.004.

References

- C. Mason, P. Dunnill, A brief definition of regenerative medicine, Regen. Med. 3 (1) (2008) 1–5.
- [2] D.L. Stocum, Stem cells in CNS and cardiac regeneration, Adv. Biochem. Eng. Biotechnol. 93 (2005) 135–159.

- [3] D. Kolber-Simonds, L. Lai, S.R. Watt, M. Denaro, S. Arn, M.L. Augenstein, J. Betthauser, D.B. Carter, J.L. Greenstein, Y. Hao, G.S. Im, Z. Liu, G.D. Mell, C.N. Murphy, K.W. Park, A. Rieke, D.J. Ryan, D.H. Sachs, E.J. Forsberg, R.S. Prather, R.J. Hawley, Production of alpha-1,3-galactosyltransferase null pigs by means of nuclear transfer with fibroblasts bearing loss of heterozygosity mutations, Proc. Natl. Acad. Sci. U. S. A. 101 (19) (2004) 7335–7340.
- [4] R.P.H. Meier, Y.D. Muller, A. Balaphas, P. Morel, M. Pascual, J.D. Seebach, L.H. Buhler, Xenotransplantation: back to the future? Transpl. Int. 31 (5) (2018) 465–477.
- [5] J.G. Mount, M. Muzylak, S. Allen, T. Althnaian, I.M. McGonnell, J.S. Price, Evidence that the canonical Wnt signalling pathway regulates deer antler regeneration, Dev. Dvn. 235 (5) (2006) 1390–1399.
- [6] E.M. Tanaka, P.W. Reddien, The cellular basis for animal regeneration, Dev. Cell 21 (1) (2011) 172–185.
- [7] S.E. Iismaa, X. Kaidonis, A.M. Nicks, N. Bogush, K. Kikuchi, N. Naqvi, R.P. Harvey, A. Husain, R.M. Graham, Comparative regenerative mechanisms across different mammalian tissues, NPJ Regen. Med. 3 (2018) 6.
- [8] A.G. Lai, A.A. Aboobaker, EvoRegen in animals: Time to uncover deep conservation or convergence of adult stem cell evolution and regenerative processes, Dev. Biol. 433 (2) (2018) 118–131.
- [9] U. Kierdorf, H. Kierdorf, T. Szuwart, Deer antler regeneration: cells, concepts, and controversies, J. Morphol. 268 (8) (2007) 726–738.
- [10] C. Li, W. Chu, The regenerating antler blastema: the derivative of stem cells resident in a pedicle stump, Front. Biosci. (Landmark Ed) 21 (2016) 455–467.
- [11] C. Li, J.M. Suttie, Deer antlerogenic periosteum: a piece of postnatally retained embryonic tissue? Anat. Embryol. (Berl.) 204 (5) (2001) 375–388.
- [12] R.J. Goss, Deer Antlers: Regeneration, Function and Evolution, Academic Press,
- 1983.
 [13] C. Li, A.J. Harris, J.M. Suttie, Tissue interactions and antlerogenesis: new findings
- revealed by a xenograft approach, J. Exp. Zool. 290 (1) (2001) 18–30. [14] C. Li, X. Gao, F. Yang, S.K. Martin, S.R. Haines, X. Deng, J. Schofield, J.A. Stanton, Development of a nude mouse model for the study of antlerogenesis—mechanism of tissue interactions and ossification pathway, J. Exp. Zool. B Mol. Dev. Evol. 312 (2) (2009) 118–135.
- [15] C. Li, C.G. Mackintosh, S.K. Martin, D.E. Clark, Identification of key tissue type for antler regeneration through pedicle periosteum deletion, Cell Tissue Res. 328 (1) (2007) 65–75.
- [16] C. Li, J.M. Suttie, Tissue collection methods for antler research, Eur. J. Morphol. 41 (1) (2003) 23–30.
- [17] H.J. Rolf, U. Kierdorf, H. Kierdorf, J. Schulz, N. Seymour, H. Schliephake, J. Napp, S. Niebert, H. Wolfel, K.G. Wiese, Localization and characterization of STRO-1 cells in the deer pedicle and regenerating antler, PLoS One 3 (4) (2008) e2064.
- [18] D.K. Berg, C. Li, G. Asher, D.N. Wells, B. Oback, Red deer cloned from antler stem cells and their differentiated progeny, Biol. Reprod. 77 (3) (2007) 384–394.
- [19] J. Price, C. Faucheux, S. Allen, Deer antlers as a model of Mammalian regeneration, Curr. Top. Dev. Biol. 67 (2005) 1–48.
- [20] C. Li, F. Yang, A. Sheppard, Adult stem cells and mammalian epimorphic regeneration-insights from studying annual renewal of deer antlers, Curr. Stem Cell Res. Ther. 4 (3) (2009) 237–251.
- [21] A. Alban, S.O. David, L. Bjorkesten, C. Andersson, E. Sloge, S. Lewis, I. Currie, A novel experimental design for comparative two-dimensional gel analysis: two-dimensional difference gel electrophoresis incorporating a pooled internal standard, Proteomics 3 (1) (2003) 36–44.
- [22] R. Diez, M. Herbstreith, C. Osorio, O. Alzate, 2-D Fluorescence Difference Gel Electrophoresis (DIGE) in Neuroproteomics, in: O. Alzate (Ed.), Neuroproteomics, 2010 Boca Raton, FL.
- [23] H. Sun, F. Yang, W. Chu, H. Zhao, C. McMahon, C. Li, Lentiviral-mediated RNAi knockdown of Cbfa1 gene inhibits endochondral ossification of antler stem cells in micromass culture, PLoS One 7 (10) (2012) e47367.
- [24] C. Li, A. Harper, J. Puddick, W. Wang, C. McMahon, Proteomes and signalling pathways of antler stem cells, PLoS One 7 (1) (2012) e30026.
- [25] Z. Dong, H. Ba, W. Zhang, D. Coates, C. Li, iTRAQ-based Quantitative Proteomic Analysis of the Potentiated and Dormant Antler Stem Cells, Int. J. Mol. Sci. 17 (11) (2016).
- [26] H. Mi, X. Huang, A. Muruganujan, H. Tang, C. Mills, D. Kang, P.D. Thomas, PANTHER version 11: expanded annotation data from Gene Ontology and Reactome pathways, and data analysis tool enhancements, Nucleic Acids Res. 45 (D1) (2017) D183–D189.
- [27] P. Shannon, A. Markiel, O. Ozier, N.S. Baliga, J.T. Wang, D. Ramage, N. Amin, B. Schwikowski, T. Ideker, Cytoscape: a software environment for integrated models of biomolecular interaction networks, Genome Res. 13 (11) (2003) 2498–2504.
- [28] G. Bindea, J. Galon, B. Mlecnik, CluePedia Cytoscape plugin: pathway insights using integrated experimental and in silico data, Bioinformatics 29 (5) (2013) 661–663.
- [29] G. Bindea, B. Mlecnik, H. Hackl, P. Charoentong, M. Tosolini, A. Kirilovsky, W.H. Fridman, F. Pages, Z. Trajanoski, J. Galon, ClueGO: a Cytoscape plug-in to decipher functionally grouped gene ontology and pathway annotation networks, Bioinformatics 25 (8) (2009) 1091–1093.
- [30] D.W. Huang, B.T. Sherman, Q. Tan, J.R. Collins, W.G. Alvord, J. Roayaei, R. Stephens, M.W. Baseler, H.C. Lane, R.A. Lempicki, The DAVID gene functional classification tool: a novel biological module-centric algorithm to functionally analyze large gene lists, Genome Biol. 8 (9) (2007) R183.
- [31] C. Li, F. Yang, G. Li, X. Gao, X. Xing, H. Wei, X. Deng, D.E. Clark, Antler regeneration: a dependent process of stem tissue primed via interaction with its enveloping skin, J. Exp. Zool. A Ecol. Genet. Physiol. 307 (2) (2007) 95–105.
- [32] P. Wang, F. Xie, J. Pan, X. Tang, Differences in the structure and osteogenesis

- capacity of the periosteum from different parts of minipig mandibles, J. Oral Maxillofac. Surg. 70 (6) (2012) 1331–1337.
- [33] Z. Lin, A. Fateh, D.M. Salem, G. Intini, Periosteum: biology and applications in craniofacial bone regeneration, J. Dent. Res. 93 (2) (2014) 109–116.
- [34] B. Almuzzaini, A.A. Sarshad, A.S. Rahmanto, M.L. Hansson, A. Von Euler, O. Sangfelt, N. Visa, A.K. Farrants, P. Percipalle, In beta-actin knockouts, epigenetic reprogramming and rDNA transcription inactivation lead to growth and proliferation defects, FASEB J. 30 (8) (2016) 2860–2873.
- [35] K. Honda, T. Yamada, R. Endo, Y. Ino, M. Gotoh, H. Tsuda, Y. Yamada, H. Chiba, S. Hirohashi, Actinin-4, a novel actin-bundling protein associated with cell motility and cancer invasion, J. Cell Biol. 140 (6) (1998) 1383–1393.
- [36] C. Lagresle-Peyrou, S. Luce, F. Ouchani, T.S. Soheili, H. Sadek, M. Chouteau, A. Durand, I. Pic, J. Majewski, C. Brouzes, N. Lambert, A. Bohineust, E. Verhoeyen, F.L. Cosset, A. Magerus-Chatinet, F. Rieux-Laucat, V. Gandemer, D. Monnier, C. Heijmans, M. van Gijn, V.A. Dalm, N. Mahlaoui, J.L. Stephan, C. Picard, A. Durandy, S. Kracker, C. Hivroz, N. Jabado, G. de Saint Basile, A. Fischer, M. Cavazzana, I. Andre-Schmutz, X-linked primary immunodeficiency associated with hemizygous mutations in the moesin (MSN) gene, J. Allergy Clin. Immunol. 138 (6) (2016) 1681–1689 e8.
- [37] S. Crunkhorn, Regenerative medicine: Inhibiting prostaglandin breakdown triggers tissue regeneration, Nat. Rev. Drug Discov. 14 (8) (2015) 526.
- [38] J. Martel-Pelletier, J.P. Pelletier, H. Fahmi, Cyclooxygenase-2 and prostaglandins in articular tissues, Semin. Arthritis Rheum. 33 (3) (2003) 155–167.
- [39] A.S. Zhu, A. Li, T.S. Ratliff, M. Melsom, L.A. Garza, After skin wounding, noncoding dsRNA coordinates prostaglandins and Wnts to promote regeneration, J. Invest. Dermatol. 137 (7) (2017) 1562–1568.
- [40] A.T.V. Ho, A.R. Palla, M.R. Blake, N.D. Yucel, Y.X. Wang, K.E.G. Magnusson, C.A. Holbrook, P.E. Kraft, S.L. Delp, H.M. Blau, Prostaglandin E2 is essential for efficacious skeletal muscle stem-cell function, augmenting regeneration and strength, Proc. Natl. Acad. Sci. U. S. A. 114 (26) (2017) 6675–6684.
- [41] S. Otsuka, T. Aoyama, M. Furu, K. Ito, Y. Jin, A. Nasu, K. Fukiage, Y. Kohno, T. Maruyama, T. Kanaji, A. Nishiura, H. Sugihara, S. Fujimura, T. Otsuka, T. Nakamura, J. Toguchida, PGE2 signal via EP2 receptors evoked by a selective agonist enhances regeneration of injured articular cartilage, Osteoarthr. Cartil. 17 (4) (2009) 529–538.
- [42] Y. Zhang, A. Desai, S.Y. Yang, K.B. Bae, M.I. Antczak, S.P. Fink, S. Tiwari, J.E. Willis, N.S. Williams, D.M. Dawson, D. Wald, W.D. Chen, Z. Wang, L. Kasturi, G.A. Larusch, L. He, F. Cominelli, L. Di Martino, Z. Djuric, G.L. Milne, M. Chance, J. Sanabria, C. Dealwis, D. Mikkola, J. Naidoo, S. Wei, H.H. Tai, S.L. Gerson, J.M. Ready, B. Posner, J.K. Willson, S.D. Markowitz, Tissue regeneration: Inhibition of the prostaglandin-degrading enzyme 15-PGDH potentiates tissue regeneration,
- Science 348 (6240) (2015) aaa2340. [43] J.C. Venter, M.D. Adams, E.W. Myers, P.W. Li, R.J. Mural, G.G. Sutton, H.O. Smith, M. Yandell, C.A. Evans, R.A. Holt, J.D. Gocayne, P. Amanatides, R.M. Ballew, D.H. Huson, J.R. Wortman, Q. Zhang, C.D. Kodira, X.H. Zheng, L. Chen, M. Skupski, G. Subramanian, P.D. Thomas, J. Zhang, G.L. Gabor Miklos, C. Nelson, S. Broder, A.G. Clark, J. Nadeau, V.A. McKusick, N. Zinder, A.J. Levine, R.J. Roberts, M. Simon, C. Slayman, M. Hunkapiller, R. Bolanos, A. Delcher, I. Dew, D. Fasulo, M. Flanigan, L. Florea, A. Halpern, S. Hannenhalli, S. Kravitz, S. Levy, C. Mobarry, K. Reinert, K. Remington, J. Abu-Threideh, E. Beasley, K. Biddick, V. Bonazzi, R. Brandon, M. Cargill, I. Chandramouliswaran, R. Charlab, K. Chaturvedi, Z. Deng, V. Di Francesco, P. Dunn, K. Eilbeck, C. Evangelista, A.E. Gabrielian, W. Gan, W. Ge, F. Gong, Z. Gu, P. Guan, T.J. Heiman, M.E. Higgins, R.R. Ji, Z. Ke, K.A. Ketchum, Z. Lai, Y. Lei, Z. Li, J. Li, Y. Liang, X. Lin, F. Lu, G.V. Merkulov, N. Milshina, H.M. Moore, A.K. Naik, V.A. Narayan, B. Neelam, D. Nusskern, D.B. Rusch, S. Salzberg, W. Shao, B. Shue, J. Sun, Z. Wang, A. Wang, X. Wang, J. Wang, M. Wei, R. Wides, C. Xiao, C. Yan, A. Yao, J. Ye, M. Zhan, W. Zhang, H. Zhang, Q. Zhao, L. Zheng, F. Zhong, W. Zhong, S. Zhu, S. Zhao, D. Gilbert, S. Baumhueter, G. Spier, C. Carter, A. Cravchik, T. Woodage, F. Ali, H. An, A. Awe, D. Baldwin, H. Baden, M. Barnstead, I. Barrow, K. Beeson, D. Busam, A. Carver, A. Center, M.L. Cheng, L. Curry, S. Danaher, L. Davenport, R. Desilets, S. Dietz, K. Dodson, L. Doup, S. Ferriera, N. Garg, A. Gluecksmann, B. Hart, J. Haynes, C. Haynes, C. Heiner, S. Hladun, D. Hostin, J. Houck, T. Howland, C. Ibegwam, J. Johnson, F. Kalush, L. Kline, S. Koduru, A. Love, F. Mann, D. May, S. McCawley, T. McIntosh, I. McMullen, M. Moy, L. Moy, B. Murphy, K. Nelson, C. Pfannkoch, E. Pratts, V. Puri, H. Qureshi, M. Reardon, R. Rodriguez, Y.H. Rogers, D. Romblad, B. Ruhfel, R. Scott, C. Sitter, M. Smallwood, E. Stewart, R. Strong, E. Suh, R. Thomas, N.N. Tint, S. Tse, C. Vech, G. Wang, J. Wetter, S. Williams, M. Williams, S. Windsor, E. Winn-Deen, K. Wolfe, J. Zaveri, K. Zaveri, J.F. Abril, R. Guigo, M.J. Campbell, K.V. Sjolander, B. Karlak, A. Kejariwal, H. Mi, B. Lazareva, T. Hatton, A. Narechania, K. Diemer, A. Muruganujan, N. Guo, S. Sato, V. Bafna, S. Istrail, R. Lippert, R. Schwartz, B. Walenz, S. Yooseph, D. Allen, A. Basu, J. Baxendale, L. Blick, M. Caminha, J. Carnes-Stine, P. Caulk, Y.H. Chiang, M. Coyne, C. Dahlke, A. Mays, M. Dombroski, M. Donnelly, D. Ely, S. Esparham, C. Fosler, H. Gire, S. Glanowski, K. Glasser, A. Glodek, M. Gorokhov, K. Graham, B. Gropman, M. Harris, J. Heil, S. Henderson, J. Hoover, D. Jennings, C. Jordan, J. Jordan, J. Kasha, L. Kagan, C. Kraft, A. Levitsky, M. Lewis, X. Liu, J. Lopez, D. Ma, W. Majoros, J. McDaniel, S. Murphy, M. Newman, T. Nguyen, N. Nguyen, M. Nodell, S. Pan, J. Peck, M. Peterson, W. Rowe, R. Sanders, J. Scott, M. Simpson, T. Smith, A. Sprague, T. Stockwell, R. Turner, E. Venter, M. Wang, M. Wen, D. Wu, M. Wu, A. Xia, A. Zandieh, X. Zhu, The sequence of the human genome, Science 291 (5507) (2001)
- [44] A.G. Gilman, G proteins: transducers of receptor-generated signals, Annu. Rev. Biochem. 56 (1987) 615–649.
- [45] L. Birnbaumer, G proteins in signal transduction, Annu. Rev. Pharmacol. Toxicol. 30 (1990) 675–705.

- [46] X. Geng, T. Xu, Z. Niu, X. Zhou, L. Zhao, Z. Xie, D. Xue, F. Zhang, C. Xu, Differential proteome analysis of the cell differentiation regulated by BCC, CRH, CXCR4, GnRH, GPCR, IL1 signaling pathways in Chinese fire-bellied newt limb regeneration, Differentiation 88 (4–5) (2014) 85–96.
- [47] L. Wattanachanya, L. Wang, S.M. Millard, W.D. Lu, D. O'Carroll, E.C. Hsiao, B.R. Conklin, R.A. Nissenson, Assessing the osteoblast transcriptome in a model of enhanced bone formation due to constitutive Gs-G protein signaling in osteoblasts, Exp. Cell Res. 333 (2) (2015) 289–302.
- [48] L. Wang, E.C. Hsiao, S. Lieu, M. Scott, D. O'Carroll, A. Urrutia, B.R. Conklin, C. Colnot, R.A. Nissenson, Loss of Gi G-protein-coupled receptor signaling in osteoblasts accelerates bone fracture healing, J. Bone Miner. Res. 30 (10) (2015) 1896–1904
- [49] S. Li, C. Yang, L. Zhang, X. Gao, X. Wang, W. Liu, Y. Wang, S. Jiang, Y.H. Wong, Y. Zhang, K. Liu, Promoting axon regeneration in the adult CNS by modulation of the melanopsin/GPCR signaling, Proc. Natl. Acad. Sci. U. S. A. 113 (7) (2016) 1937–1042
- [50] K. Zuo, D. Kuang, Y. Wang, Y. Xia, W. Tong, X. Wang, Y. Chen, Y. Duan, G. Wang, SCF/c-kit transactivates CXCR4-serine 339 phosphorylation through G proteincoupled receptor kinase 6 and regulates cardiac stem cell migration, Sci. Rep. 6 (2016) 26812.
- [51] A. Mogha, B.L. Harty, D. Carlin, J. Joseph, N.E. Sanchez, U. Suter, X. Piao, V. Cavalli, K.R. Monk, Gpr126/Adgrg6 has Schwann cell autonomous and nonautonomous functions in peripheral nerve injury and repair, J. Neurosci. 36 (49) (2016) 12351–12367.
- [52] M. Scolz, P.O. Widlund, S. Piazza, D.R. Bublik, S. Reber, L.Y. Peche, Y. Ciani, N. Hubner, M. Isokane, M. Monte, J. Ellenberg, A.A. Hyman, C. Schneider, A.W. Bird, GTSE1 is a microtubule plus-end tracking protein that regulates EB1dependent cell migration, PLoS One 7 (12) (2012) e51259.
- [53] B. Chen, W.H. Piel, L. Gui, E. Bruford, A. Monteiro, The HSP90 family of genes in the human genome: insights into their divergence and evolution, Genomics 86 (6) (2005) 627–637.
- [54] S.E. Jackson, Hsp90: structure and function, Top, Curr. Chem. 328 (2013) 155–240.
- [55] D.R. Bublik, M. Scolz, G. Triolo, M. Monte, C. Schneider, Human GTSE-1 regulates p21(CIP1/WAF1) stability conferring resistance to paclitaxel treatment, J. Biol. Chem. 285 (8) (2010) 5274–5281.
- [56] Q. Guo, D. Wang, Z. Liu, C. Li, Effects of p21 gene down-regulation through RNAi on Antler stem cells in vitro, PLoS One 10 (8) (2015) e0134268.
- [57] M. Janco, A. Kalyva, B. Scellini, N. Piroddi, C. Tesi, C. Poggesi, M.A. Geeves, Alpha-Tropomyosin with a D175N or E180G mutation in only one chain differs from tropomyosin with mutations in both chains, Biochemistry 51 (49) (2012) 9880–9890.
- [58] P.A. Huber, C.S. Redwood, N.D. Avent, M.J. Tanner, S.B. Marston, Identification of functioning regulatory sites and a new myosin binding site in the C-terminal 288 amino acids of caldesmon expressed from a human clone, J. Muscle Res. Cell Motil. 14 (4) (1993) 385–391.
- [59] E. Kremneva, O. Nikolaeva, R. Maytum, A.M. Arutyunyan, S.Y. Kleimenov, M.A. Geeves, D.I. Levitsky, Thermal unfolding of smooth muscle and nonmuscle tropomyosin alpha-homodimers with alternatively spliced exons, FEBS J. 273 (3) (2006) 588–600.
- [60] M.A. Lizarbe, J.I. Barrasa, N. Olmo, F. Gavilanes, J. Turnay, Annexin-phospholipid interactions. Functional implications, Int. J. Mol. Sci. 14 (2) (2013) 2652–2683.
- [61] U. Roostalu, U. Strahle, In vivo imaging of molecular interactions at damaged sarcolemma, Dev. Cell 22 (3) (2012) 515–529.
- [62] N.J. Lennon, A. Kho, B.J. Bacskai, S.L. Perlmutter, B.T. Hyman, R.H. Brown Jr., Dysferlin interacts with annexins A1 and A2 and mediates sarcolemmal wound-healing, J. Biol. Chem. 278 (50) (2003) 50466–50473.
- [63] D.E. Clark, C. Li, W. Wang, S.K. Martin, J.M. Suttie, Vascular localization and proliferation in the growing tip of the deer antler, Anat Rec A Discov Mol Cell Evol Biol 288 (9) (2006) 973–981.
- [64] X. Huang, J.P. Saint-Jeannet, Induction of the neural crest and the opportunities of life on the edge, Dev. Biol. 275 (1) (2004) 1–11.
- [65] J. Price, S. Allen, Exploring the mechanisms regulating regeneration of deer antlers, Philos. Trans. R. Soc. Lond. Ser. B Biol. Sci. 359 (1445) (2004) 809–822.

- [66] U. Kierdorf, H. Kierdorf, Pedicle and first antler formation in deer: Anatomical, histological, and developmental aspects, Z. Jagdwiss. 48 (1) (2002) 22–34.
- [67] J. Mount, M. Muzylak, S. Allen, S. Okushima, T. Althnaian, I. McGonnell, J. Price, Antlers may regenerate from persistent neural crestlike stem cells, Advances in Deer Biology, 2006, p. 161.
- [68] J.P. Thiery, H. Acloque, R.Y. Huang, M.A. Nieto, Epithelial-mesenchymal transitions in development and disease, Cell 139 (5) (2009) 871–890.
- [69] L. Kerosuo, M. Bronner-Fraser, What is bad in cancer is good in the embryo: Importance of EMT in neural crest development, Semin. Cell Dev. Biol. 23 (3) (2012) 320–332.
- [70] M.A. Nieto, The snail superfamily of zinc-finger transcription factors, Nat. Rev. Mol. Cell Biol. 3 (3) (2002) 155–166.
- [71] D.T. Wang, W.H. Chu, H.M. Sun, H.X. Ba, C.Y. Li, Expression and functional analysis of tumor-related factor S100A4 in Antler stem cells, J. Histochem. Cytochem. 65 (10) (2017) 579–591.
- [72] H. Takigawa, Y. Kitadai, K. Shinagawa, R. Yuge, Y. Higashi, S. Tanaka, W. Yasui, K. Chayama, Mesenchymal stem cells induce epithelial to mesenchymal transition in colon cancer cells through direct cell-to-cell contact, Neoplasia 19 (5) (2017) 429-438
- [73] M. Schneider, J.L. Hansen, S.P. Sheikh, S100A4: a common mediator of epithelial-mesenchymal transition, fibrosis and regeneration in diseases? J. Mol. Med. (Berl.) 86 (5) (2008) 507–522.
- [74] J.Y. Hung, M.C. Yen, S.F. Jian, C.Y. Wu, W.A. Chang, K.T. Liu, Y.L. Hsu, I.W. Chong, P.L. Kuo, Secreted protein acidic and rich in cysteine (SPARC) induces cell migration and epithelial mesenchymal transition through WNK1/snail in non-small cell lung cancer, Oncotarget 8 (38) (2017) 63691–63702.
- [75] C.H. Chang, M.C. Yen, S.H. Liao, Y.L. Hsu, C.S. Lai, K.P. Chang, Y.L. Hsu, Secreted protein acidic and rich in cysteine (SPARC) enhances cell proliferation, migration, and epithelial mesenchymal transition, and SPARC expression is associated with tumor grade in head and neck cancer, Int. J. Mol. Sci. 18 (7) (2017).
- [76] D. Tang, J. Zhang, Z. Yuan, H. Zhang, Y. Chong, Y. Huang, J. Wang, Q. Xiong, S. Wang, Q. Wu, Y. Tian, Y. Lu, X. Ge, W. Shen, D. Wang, PSC-derived Galectin-1 inducing epithelial-mesenchymal transition of pancreatic ductal adenocarcinoma cells by activating the NF-kappaB pathway, Oncotarget 8 (49) (2017) 86488–86502.
- [77] M.L. Bacigalupo, M. Manzi, M.V. Espelt, L.D. Gentilini, D. Compagno, D.J. Laderach, C. Wolfenstein-Todel, G.A. Rabinovich, M.F. Troncoso, Galectin-1 triggers epithelial-mesenchymal transition in human hepatocellular carcinoma cells, J. Cell. Physiol. 230 (6) (2015) 1298–1309.
- [78] K.H. Chow, H.J. Park, J. George, K. Yamamoto, A.D. Gallup, J.H. Graber, Y. Chen, W. Jiang, D.A. Steindler, E.G. Neilson, B.Y.S. Kim, K. Yun, S100A4 is a biomarker and regulator of glioma stem cells that is critical for mesenchymal transition in glioblastoma, Cancer Res. 77 (19) (2017) 5360–5373.
- [79] J.M. Dave, K.J. Bayless, Vimentin as an integral regulator of cell adhesion and endothelial sprouting, Microcirculation 21 (4) (2014) 333–344.
- [80] P. Sharma, The Influence of Vimentin Intermediate Filaments on Human Mesenchymal Stem Cell Response to Physical Stimuli, (2017).
- [81] H. Wang, B. Huang, B.M. Li, K.Y. Cao, C.Q. Mo, S.J. Jiang, J.C. Pan, Z.R. Wang, H.Y. Lin, D.H. Wang, S.P. Qiu, ZEB1-mediated vasculogenic mimicry formation associates with epithelial-mesenchymal transition and cancer stem cell phenotypes in prostate cancer, J. Cell. Mol. Med. 22 (8) (2018) 3768–3781.
- [82] N.J. Kruger, A. von Schaewen, The oxidative pentose phosphate pathway: structure and organisation, Curr. Opin. Plant Biol. 6 (3) (2003) 236–246.
- [83] E. Melendez-Hevia, A. Isidoro, The game of the pentose phosphate cycle, J. Theor. Biol. 117 (2) (1985) 251–263.
- [84] C.D. Mol, J.M. Harris, E.M. McIntosh, J.A. Tainer, Human dUTP pyrophosphatase: uracil recognition by a beta hairpin and active sites formed by three separate subunits, Structure 4 (9) (1996) 1077–1092.
- [85] J.D. Pollack, M.V. Williams, R.N. McElhaney, The comparative metabolism of the mollicutes (Mycoplasmas): the utility for taxonomic classification and the relationship of putative gene annotation and phylogeny to enzymatic function in the smallest free-living cells, Crit. Rev. Microbiol. 23 (4) (1997) 269–354.